Maternal *Smc3* protects the integrity of the zygotic genome through DNA replication and mitosis

Wei-Ting Yueh[1], Vijay Pratap Singh[1], and Jennifer L. Gerton[1,2*]

[1]Stowers Institute for Medical Research, Kansas City, MO, 64110

[2]Department of Biochemistry and Molecular Biology, University of Kansas Medical Center, Kansas City, KS 66160

[*]Corresponding author

Correspondence: Jennifer L. Gerton, PhD

Stowers Institute for Medical Research
1000 E. 50th St
Kansas City, MO 64110 USA
Tel: 816-926-4443
Email: jeg@stowers.org

Keywords: cohesin, SMC3, spontaneous DNA damage, chromosome segregation, micronuclei, mouse, zygote, juvenile, maternal effect gene, developmental competence

© 2021. Published by The Company of Biologists Ltd.
This is an Open Access article distributed under the terms of the Creative Commons Attribution License (http://creativecommons.org/licenses/by/4.0), which permits unrestricted use, distribution and reproduction in any medium provided that the original work is properly attributed.

Development • Accepted manuscript

Summary Statement: This study demonstrates at a molecular level how maternally provided SMC3 supports the first round of DNA replication and chromosome segregation in the zygote to enable successful embryogenesis.

ABSTRACT

Aneuploidy is frequently observed in oocytes and early embryos, begging the question of how genome integrity is monitored and preserved during this critical period. SMC3 is a subunit of the cohesin complex that supports genome integrity, but its role in maintaining the genome in this window of mammalian development is unknown. We discovered that although depletion of *Smc3* following meiotic S phase in mouse oocytes allowed accurate meiotic chromosome segregation, adult females were infertile. We provide evidence that DNA lesions accumulated following S phase in SMC3-deficient zygotes, followed by mitosis with lagging chromosomes, elongated spindles, micronuclei, and arrest at the 2-cell stage. Remarkably, although centromeric cohesion was defective, the dosage of SMC3 was sufficient to enable embryogenesis in juvenile mutant females. Our findings suggest that despite previous reports of aneuploidy in early embryos, chromosome missegregation in zygotes halts embryogenesis at the 2-cell stage. *Smc3* is a maternal gene with essential functions in repair of spontaneous damage associated with DNA replication and subsequent chromosome segregation in zygotes, making cohesin a key protector of the zygotic genome.

Development • Accepted manuscript

INTRODUCTION

Infertility impacts the psychological well-being and economic status, mental health, sexual and marital relationships, and quality of life of women and couples (Luk and Loke, 2015, Namdar et al., 2017) with 4.65 million couples experiencing infertility in the US in 2013 (Thoma et al., 2013). Among numerous factors, oocyte quality contributes significantly to infertility. Female reproduction is profoundly affected by age (Hassold and Hunt, 2001, Hunt, 2017); fertility starts to decline in the mid-thirties and accelerates thereafter. Women are born with all the eggs for their lifetime and these eggs decrease in quality and quantity with age. While faulty meiosis is a major contributor to female infertility, early embryonic failure also contributes, making it desirable to have visual markers for in vitro fertilization that indicate successful outcomes. Many factors essential for developmental competence are loaded into oocytes, so called maternal effect genes.

Chromosome segregation during early development in mammals is highly error prone and aneuploidy abounds in oocytes and early embryos (Hassold and Hunt, 2001, Vázquez-Diez and FitzHarris, 2018, Radonova et al., 2019, Pauerova et al., 2020), underscoring the need to understand how the genome is transmitted from one generation to the next. Cohesin is a genome maintenance protein complex required for successful meiosis and mitosis. Cohesin is a ring-shaped multi-protein complex that plays multiple critical functions in sister chromatid cohesion, DNA damage repair, higher-order chromosome structure, and gene expression including epigenetic reprogramming. The cohesin ring consists of four modular subunits: SMC1α or β, SMC3, RAD21 or REC8 (Scc1), and Stromalin 1 (STAG1) or Stromalin 2 (STAG2). Cohesin

Development • Accepted manuscript

holds sister chromatid pairs together from DNA replication until mitosis (Uhlmann and Nasmyth, 1998, Losada et al., 1998, Murayama et al., 2018, Nasmyth and Haering, 2005). The biorientation of sisters at metaphase requires cohesion. Cohesion can be established between sister chromatids during DNA replication, and in G2 following a double-strand break (DSB) (Uhlmann and Nasmyth, 1998, Ström and Sjögren, 2005). Cohesin enforces DSB repair from the sister template. Other SMC protein complexes include condensin and SMC5/6. SMC5/6 plays roles in DNA repair, whereas condensin is critical for condensation of chromosomes (Aragón, 2018, Thadani and Uhlmann, 2015). A complete picture of how the genome is transmitted from the germline into the next generation requires the field to understand how SMC complexes support the maintenance of the genome during this critical transition.

The molecular events underlying the earliest stages of embryogenesis and how they are linked to the previous meiosis are foundational to development. Relatively few genes have been demonstrated to be essential in mouse oocytes to support blastocyst development, so called maternal effect genes, although more are suspected to exist (Kim and Lee, 2014, Condic, 2016). Knowledge of the working mechanisms of maternal effect genes is essential to understand developmental competence. Most maternal effect genes have been shown to support imprinting and zygotic genome activation. The RAD21 subunit of cohesin and the cohesin associated DNA binding protein CCCTC-binding factor (CTCF) have both been shown to act as maternal effect genes, with critical roles in reprogramming and gene expression in the embryo (Ladstätter and Tachibana-Konwalski, 2016, Fedoriw et al., 2004, Wan et al., 2008). *Smc5* depletion in oocytes with the *Zp3-cre* driver leads to segregation incompetent bivalents during

Development • Accepted manuscript

meiosis I (Hwang et al., 2017). Depletion of cohesin subunits in oocytes may leave cohesin associated with chromosomes since sister chromatid cohesion is established during pre-meiotic S phase and cohesin does not turnover, although age-associated erosion can lead to aneuploidy (Burkhardt et al., 2016, Tachibana-Konwalski et al., 2010, Hodges et al., 2005). Furthermore, the dosage of cohesin can affect chromosome structure and behavior in mouse oocytes (Murdoch et al., 2013). Among the four modular subunits, SMC3 is the only subunit that exists in all cohesin complexes, so its ablation will affect all mitotic and meiotic complexes. Our previous study indicates that depletion of *Histone deacetylase 8* (*Hdac8*), a key recycling factor for SMC3, in mouse oocytes does not block embryogenesis (Singh et al., 2019). How *Smc3* contributes to genome integrity and transmission in mouse oocytes and zygotes has not been examined.

We demonstrate herein that *Smc3* in oocytes is required for female fertility and integrity of the zygotic genome. We report that depletion of SMC3 in mouse oocytes causes infertility due to failed embryogenesis. Unlike most maternal effect genes characterized to date, *Smc3* is required to maintain the integrity and segregation of zygotic chromosomes. Depletion of SMC3 in oocytes leads to a series of molecular events that include: 1) persistence of DNA damage following DNA replication, 2) cohesion defects and lagging chromosomes at the first cleavage, 3) sister chromatid missegregation with elongated spindles, 4) micronuclei, and 5) arrest at the 2-cell stage. Remarkably, and in contrast to adult females, the dosage of maternal SMC3 in juvenile mutant females is sufficient to support developmental competence, despite compromised centromeric cohesion in the zygote. We propose that maternal SMC3 in

Development • Accepted manuscript

the oocyte is required to support the integrity and transmission of the zygotic genome following DNA replication. Despite the high rates of aneuploidy observed during early embryogenesis, these results highlight the fundamental importance of euploidy at the 2-cell stage. Furthermore, our study suggests zygotes can bypass chromosome cohesion defects and chromosome missegregation at the first cleavage, but aneuploidy may be a deal breaker for progression of 2-cell stage embryos.

RESULTS

Conditional deletion of maternal *Smc3* results in female infertility

To study the role of *Smc3* in female germ cells, we utilized a conditional knockout strategy based on two Cre drivers. *Gdf9-iCre* and *Zp3-Cre* each express Cre recombinase in oocytes at different stages of development (Lan et al., 2004). Whereas *Zp3-Cre* expression in oocytes by postnatal day 3 (P3) is uncontested, the expression of *Gdf9-iCre* at 13.5 dpc has been debated (Ladstätter and Tachibana-Konwalski, 2016, Lan et al., 2004). To detect the timing of *Gdf9-iCre* expression, we examined female gonads with a LacZ reporter. We observed *β-gal* staining in female gonads at 13.5 dpc (**Figure S1**), suggesting that *Gdf9-iCre* deletes the floxed-*Smc3* allele in oocytes during pre-meiotic DNA replication. Next, we validated the efficiency of the Cre recombinases in Western blots detecting SMC3 protein levels in $Smc3^{fl/fl}$;*Gdf9-iCre* and $Smc3^{fl/fl}$;*Zp3-Cre* oocytes along with wild type ($Smc3^{fl/fl}$) controls. The level of SMC3 significantly decreased 54% and 77% in $Smc3^{fl/fl}$;*Gdf9-iCre* and $Smc3^{fl/fl}$;*Zp3-Cre* germinal vesicle (GV) stage oocytes respectively, compared to controls (**Figure S2A-C**), indicating the

Development • Accepted manuscript

conditional gene knockout (cKO) strategy was successful, but Smc3 protein persists after gene deletion.

We next asked whether deletion of *Smc3* affects female fertility by carrying out a breeding trial. *Smc3*$^{fl/fl}$*;Gdf9-iCre* and *Smc3*$^{fl/fl}$*;Zp3-Cre* adult female mice were both sterile (**Figure 1A, Table 1**). Although there is variation among individuals, the heterozygous knockout *Smc3*$^{+/fl}$ *Zp3-Cre* female mice remain fertile. This indicates that a single copy of *Smc3* is sufficient to maintain developmentally competent oocytes. The level of SMC3 in heterozygotes is comparable to *cKO* and 66% lower than controls (**Figure S2C**). However, protein levels measured by Western blot may be an imperfect indicator of function. Overall, we conclude that maternal *Smc3* is required in mouse oocytes for female fertility.

Maternal *Smc3* is essential for embryogenesis

We next examined how deletion of *Smc3* in oocytes blocks reproduction. Based on female infertility with both *Gdf9-iCre and Zp3-Cre* drivers, we asked whether loss of *Smc3* impacts ovarian reserve by scoring the number of follicles in ovaries. We performed H&E staining on tissue sections of ovaries from adult female mice without hormone stimulation. Corpus lutea were observed in *Smc3*$^{fl/fl}$, *Smc3*$^{fl/fl}$*;Gdf9-iCre* and *Smc3*$^{fl/fl}$*;Zp3-Cre* female mice, suggesting these animals ovulate, and ruling out lack of ovulation as an explanation for sterility (**Figure S3A**). Furthermore, the total number of follicles is comparable in adult *Smc3*$^{fl/fl}$, *Smc3*$^{fl/fl}$*;Gdf9-iCre* and *Smc3*$^{fl/fl}$*;Zp3-Cre* female mice (**Figure S3A-B**), suggesting differences in ovarian reserve do not account for

Development • Accepted manuscript

infertility. Furthermore, ovaries from *Smc3*$^{fl/fl}$*;Gdf9-iCre* and *Smc3*$^{fl/fl}$*;Zp3-Cre* female mice contain a higher ratio of secondary and antral follicles (**Figure S3C**), suggesting that follicle maturation is not compromised but instead appears to be accelerated. Although we cannot explain why loss of *Smc3* would accelerate follicle maturation, our results suggest that loss of *Smc3* does not compromise fertility via depletion of the ovarian reserve. Next, we examined whether maternal *Smc3* in oocytes was required for meiosis. Both *Smc3*$^{fl/fl}$*;Gdf9-iCre* and *Smc3*$^{fl/fl}$*;Zp3-Cre* metaphase II oocytes had visibly normal meiotic spindles (**Figure 1B**). We further asked whether loss of *Smc3* caused aneuploidy in oocytes. To measure ploidy, we performed chromosome spreads in metaphase I and metaphase II oocytes. There were no obvious defects in chromosome structure in *Smc3*$^{fl/fl}$*;Gdf9-iCre* and *Smc3*$^{fl/fl}$*;Zp3-Cre* oocytes **(Figure 1C, Figure S4**). Furthermore, we observed a normal number of chromosome pairs in *Smc3*$^{fl/fl}$*;Gdf9-iCre* and *Smc3*$^{fl/fl}$*;Zp3-Cre* metaphase II oocytes **(Figure 1D**). Despite the differences in timing of the cre drivers, in both cases the levels of SMC3 in the oocytes appear to be sufficient for chromosome segregation during meiosis.

Next, we asked whether loss of *Smc3* impacts embryogenesis. Zygotes derived from *Smc3*$^{fl/fl}$*, Smc3*$^{fl/fl}$*;Gdf9-iCre,* and *Smc3*$^{fl/fl}$*;Zp3-Cre* female mice crossed with wild type males were isolated and cultured *in vitro*. Because the phenotype of zygotes is dominated by proteins inherited from the oocyte, and transcription is negligible prior to the first mitotic division **(Hamatani et al., 2004, Aoki et al., 1997)**, we designate the genotype of the zygote according to the maternal allele. Zygotes from *Smc3*$^{fl/fl}$*;Gdf9-iCre* and *Smc3*$^{fl/fl}$*;Zp3-Cre* adult female mice arrested predominantly at the 2-cell stage (**Figure 1E, Table 2**). *Smc3*$^{fl/fl}$*;Gdf9-iCre* and *Smc3*$^{fl/fl}$*;Zp3-Cre* embryos failed to mature

Development • Accepted manuscript

to morula and blastocyst. Since the *Smc3*$^{fl/fl}$*;Gdf9-iCre* and *Smc3*$^{fl/fl}$*;Zp3-Cre* zygotes shared the same arrest phenotype, together they provide experimental replication. Moving forward, we focus on zygotes from the *Smc3*$^{fl/fl}$*;Zp3-Cre* driver because the *Zp3-Cre* driver is the standard driver used to study maternal effect genes. Hereafter for simplicity, we refer to *Smc3*$^{fl/fl}$*;Zp3-Cre* zygotes as *Smc3*$^{\Delta/\Delta}$ zygotes, recognizing that gene deletion leads to protein depletion. Our findings strongly suggest that depletion of maternal SMC3 in oocytes causes infertility by impacting embryogenesis, not oogenesis.

Spontaneous DNA damage following DNA replication persists in *Smc3*$^{\Delta/\Delta}$ *cKO* zygotes

To further examine how depletion of maternal *S*MC3 affects embryogenesis, we monitored DNA damage in different phases of the zygote cell cycle (**Figure 2A**). *Zp3-cre* mediated deletion of *Rad21*, a somatic-specific cohesin subunit, leads to unrepaired paternal DNA lesions derived from paternal reprogramming in G1 phase zygotes (Ladstätter and Tachibana-Konwalski, 2016), preventing examination of DNA damage and chromosome segregation at later stages of embryogenesis. DNA lesions were quantified based on γH2AX foci. In contrast to RAD21 depletion, DNA lesions were similar in *Smc3*$^{fl/fl}$ and *Smc3*$^{\Delta/\Delta}$ G1 phase zygotes (**Figure 2B-C**). The SMC3 subunit can be recycled via an acetylation/deacetylation mechanism from one cell cycle to the next (Deardorff et al., 2012, Xiong et al., 2010, Borges et al., 2010, Beckouët et al., 2010). Our results suggest that the recycling of SMC3 is sufficient for the repair of DNA lesions associated with paternal genome reprogramming in *Smc3*$^{\Delta/\Delta}$ G1 phase zygotes.

Development • Accepted manuscript

DNA replication generates DNA lesions such as DSBs (Arnaudeau et al., 2001). Spontaneous DNA lesions were observed during S phase in both wild type and mutant zygotes (**Figure 2D-E**), as expected. However, while DNA lesions following S phase were detected at low levels in *Smc3*$^{fl/fl}$ zygotes, indicating repair, these lesions persisted in *Smc3*$^{\Delta/\Delta}$ G2 phase zygotes (**Figure 2F-G**). Since we did not induce exogenous DNA damage, our findings strongly suggest that DNA lesions were produced spontaneously during S phase. Therefore, we speculate that maternal *Smc3* is required for the repair of spontaneous DNA lesions that arise during DNA replication, as postulated based on work in budding yeast (Ström and Sjögren, 2005).

To further examine the persistent DNA lesions in G2 phase zygotes, we probed for single-stranded DNA (ssDNA), which is generated during DNA replication. We found that RPA70, a marker of ssDNA, was significantly elevated in *Smc3*$^{\Delta/\Delta}$ G2 phase zygotes (**Figure 3A-B**). While ssDNA can be generated from either active transcription or replication, transcription is negligible in mouse zygotes (Aoki et al., 1997, Jukam et al., 2017). Therefore, ssDNA is predicted to derive primarily from DNA replication. Our data suggest that maternal *Smc3* is required to complete repair events associated with DNA replication in zygotes.

Homologous recombination is a common method used to restart stalled replication forks (Arnaudeau et al., 2001). We investigated whether RAD51 persists into G2 phase when SMC3 is depleted. We observed a significantly higher incidence of RAD51 foci in *Smc3*$^{\Delta/\Delta}$ zygotes (**Figure 3C-D**), consistent with the γH2AX data, and demonstrating that accumulation of DNA lesions in *Smc3*$^{\Delta/\Delta}$ zygotes coincides with the accumulation of homologous recombination proteins. Our findings suggest that maternal

Development • Accepted manuscript

SMC3 is necessary to complete the repair of spontaneous DNA damage from S phase in zygotes but is not essential for the recruitment of homologous recombination machinery.

Deletion of maternal *Smc3* leads to lagging chromosomes, loss of cohesion, and micronuclei during the 1st mitotic division

The first detectable phenotype following loss of *Smc3* in oocytes is persistent DNA damage in G2-phase zygotes. However, zygotes complete the first mitotic division. We next asked why $Smc3^{\Delta/\Delta}$ embryos arrest at the 2-cell stage. Although the 2-cell stage is a common arrest point in mouse embryo development, the checkpoints involved are not well characterized (Zanoni et al., 2009). Because zygotic genome activation (ZGA) occurs late in the 2-cell stage in mouse, faulty ZGA can lead to arrest (Schultz, 2002, Schultz, 1993). Since cohesin may contribute to ZGA in zebrafish (Meier et al., 2018), we examined whether loss of maternal *Smc3* is required for ZGA in mice. We measured global RNA transcription in $Smc3^{\Delta/\Delta}$ embryos at the 2-cell stage using a 5-Ethynyl uridine (5-EU) click-iT assay. In this assay, G2 phase zygotes and 2-cell stage embryos were pulse labelled with 5-EU, which incorporates into nascent RNA and can be quantified via fluorescence (see Materials and Methods). The signal was comparable between $Smc3^{fl/fl}$ and $Smc3^{\Delta/\Delta}$ 2-cell stage embryos (**Figure S5**). Although we did not determine whether the zygotic transcriptome was affected, ZGA-associated nascent transcription occurs with normal timing and to grossly normal levels in $Smc3^{\Delta/\Delta}$ embryos, suggesting ZGA can initiate.

Development • Accepted manuscript

Micronuclei are a hallmark of genome instability (Soto et al., 2018). Micronuclei often form when a chromosome or fragment fails to incorporate into the daughter nucleus during cell division. We asked whether depletion of maternal SMC3 resulted in micronuclei during the first zygotic division, detected by DNA staining in 2-cell stage embryos. Remarkably, we found that *Smc3*$^{\Delta/\Delta}$ embryos had significantly more micronuclei than *Smc3*$^{fl/fl}$ embryos (**Figure 4A-B**). This strongly suggested that loss of maternal *Smc3* in the oocyte resulted in chromosome instability during the first mitotic division. To further examine the formation of micronuclei, we used live-cell imaging. DNA in zygotes was stained with the low cell-toxicity SIR-DNA dye and imaged every 3 minutes by spinning disc confocal microscopy. This allowed us to visualize the entire process of chromosome segregation during the first mitotic division in unperturbed zygotes (**Movie 1 (WT), Movie 2 (*Smc3*$^{\Delta/\Delta}$), Figure 4C-E**). The morphology of sister chromatids in *Smc3*$^{\Delta/\Delta}$ zygotes during metaphase appeared more stretched, consistent with reduced centromeric cohesion (**Figure 4C-D**). Moreover, we observed lagging chromosomes during anaphase that formed a micronucleus (**Figure 4E**). In all 20 movies of *Smc3*$^{\Delta/\Delta}$ embryos lagging chromosomes were observed, as compared to 1 in 37 movies of *Smc3*$^{fl/fl}$ embryos. We speculate that weakened centromeric cohesion results in merotelic kinetochore attachments with kinetochores attached to microtubules from both spindle poles, a configuration that evades detection by the spindle assembly checkpoint, culminating in lagging chromosomes that form micronuclei (Haarhuis et al., 2013, Thompson and Compton, 2011). Our results demonstrate that maternal *Smc3* is required for accurate chromosome segregation during the first mitotic division.

Development • Accepted manuscript

Importantly, chromosome missegregation and aneuploidy precede ZGA and the 2-cell arrest.

Cohesin is well-known for its role in sister chromatid cohesion that facilitates biorientation and chromosome segregation. Since our live-cell imaging revealed lagging chromosomes in *Smc3*$^{\Delta/\Delta}$ zygotes, we next asked whether loss of maternal *Smc3* affected sister chromatid cohesion. To achieve this, we induced metaphase arrest with the pharmacological anaphase-promoting complex/cyclosome (APC/C) inhibitor proTAME and then examined centromeres and spindles. We observed a complete loss of sister chromatid cohesion and sister chromatid separation in all *Smc3*$^{\Delta/\Delta}$ zygotes (n=21), and maintenance in all *Smc3*$^{fl/fl}$ zygotes (n=30) (**Figure 4F**). Since precocious separation of whole chromosomes was not apparent in live-cell imaging of unperturbed mutant zygotes, we suggest that proTAME exacerbates the weakened centromeric cohesion observed in live-cell imaging due to prolonged metaphase arrest with intact microtubules generating cohesion fatigue and precocious sister separation in *Smc3*$^{\Delta/\Delta}$ zygotes. We conclude that maternal SMC3 is required in zygotes to create robust sister chromatid cohesion and prevent lagging chromosomes, micronuclei formation, and aneuploidy.

We investigated whether a DNA damage checkpoint is activated in *Smc3*$^{\Delta/\Delta}$ embryos at the 2-cell stage. To examine the canonical ATR and ATM checkpoints at the 2-cell stage, we labeled Chk1 and phospho-ATM (p-ATM), respectively (**Figure S6**). We first validated the antibodies by introducing replication stress using hydroxyurea (HU) treatment in wild type G2 phase zygotes. We found that Chk1 increased in G2 phase zygotes while p-ATM remained low (**Figure S6A-B**). Although we did not detect p-ATM

Development • Accepted manuscript

signal in G2 phase zygotes with HU treatment, this antibody has been validated in our lab in mouse placental tissue in a recent study (Singh et al., 2020). We next examined Chk1 and p-ATM levels in 2-cell stage embryos. Neither Chk1 nor p-ATM increased at the 2-cell stage in *Smc3*$^{\Delta/\Delta}$ embryos, suggesting the canonical ATM and ATR checkpoints are not activated (**Figure S6C-D**). However, checkpoints in early embryogenesis are weak or may be noncanonical (Conn et al., 2004, Vázquez-Diez et al., 2019, Satish Kumar et al., 2007, Kato and Tsunoda, 1992). Nonetheless, aneuploidy at the 2-cell stage is not tolerated as embryos do not progress to further developmental stages (Pauerova et al., 2020), suggesting aneuploidy (i.e. micronuclei) underpins the 2-cell arrest in the *Smc3*$^{\Delta/\Delta}$ embryos.

Developmental competence remains intact in mutant juveniles

If persistent DNA damage and aneuploidy underpin the 2-cell arrest, then rescuing this single round of DNA repair and chromosome segregation may permit embryogenesis, once *Smc3* can be expressed from the paternal genome during ZGA. To determine if rescue could be achieved, we delivered exogeneous *Smc3 mRNA* into *Smc3*$^{\Delta/\Delta}$ zygotes using microinjection (**Figure 5A-B)** prior to S phase. While all mock-injected *Smc3*$^{\Delta/\Delta}$ zygotes arrested at either the zygote or 2-cell stage (31 total), ~22% of microinjected mutant zygotes (9 in 44 embryos) continued past the 2-cell stage, 6 embryos successfully matured to a morula, and 2 matured to a blastocyst (**Figure 5C, Table 3**). Therefore, our data suggest that increased levels of SMC3 in zygotes enable the first mitosis and rescue embryogenesis. Microinjection is a challenging method; the imperfect rescue could arise from several factors, including 1) heterogeneity in the

Development • Accepted manuscript

timing of mating among different female mice, such that a few zygotes enter S phase prior to microinjection, although the time was selected based on staging from Figure 2, 2) insufficient translation of SMC3 protein in some zygotes. However, the rescue of embryogenesis in a subset of zygotes is consistent with the idea that sufficient SMC3 provided in the correct time window can enable developmental competence.

In addition to microinjection, we asked whether endogenous SMC3 protein could rescue the 2-cell arrest. We hypothesized that SMC3 protein levels in oocytes may decline starting at P3 with induction of the *Zp3-Cre* driver, and continue until sexual maturity, leading to a gradual loss of developmental competence. If true, juvenile females might have more SMC3 protein, which would enable the first mitotic division and developmental competence. We asked whether oocytes from juvenile $Smc3^{\Delta/\Delta}$ female mice were developmentally competent. Because most mouse strains reach sexual maturity at 4-7 weeks of age, we could not conduct a breeding trial. Instead, 3-4-week-old juvenile $Smc3^{\Delta/\Delta}$ female mice were treated with hormones for superovulation, followed by mating, zygote collection and culture *in vitro*. Remarkably, zygotes from juveniles matured to blastocysts (**Figure 6A, Table 4**). Also, the level of SMC3 in juvenile $Smc3^{\Delta/\Delta}$ GV stage oocytes was comparable to $Smc3^{fl/fl}$ levels by Western blot analysis (**Figure S7A-B**). Therefore, our data strongly suggest that the dosage of maternal SMC3 in oocytes declines between the juvenile and sexually mature stages in the mutant. Increased levels of SMC3 in the juvenile-derived oocytes enable successful chromosome segregation at the first mitosis such that developmental competence is achieved.

Development • Accepted manuscript

We then asked whether levels of SMC3 in juveniles were sufficient for repair of DNA lesions in *Smc3*$^{\Delta/\Delta}$ zygotes. We quantified γH2AX foci in juvenile-derived *Smc3*$^{fl/fl}$ and *Smc3*$^{\Delta/\Delta}$ zygotes in G2 phase (**Figure 6B-C**). Surprisingly, we found that the paternal DNA lesions increased in zygotes derived from *Smc3*$^{fl/fl}$ juvenile females, compared to mature females, suggesting either a general insufficiency of repair or an elevation in the incidence of lesions. Paternal DNA lesions were further increased in zygotes derived from juvenile *Smc3*$^{\Delta/\Delta}$ females, whereas maternal DNA lesions showed no difference, suggesting a partial rescue. To examine whether DNA repair machinery is affected in zygotes derived from juvenile *Smc3*$^{\Delta/\Delta}$ females, we quantified RAD51 foci as described previously (**Figure 6D-E**). RAD51 foci were similar in zygotes derived from juvenile and mature *Smc3*$^{fl/fl}$ females. However, RAD51 foci were elevated in zygotes derived from juvenile *Smc3*$^{\Delta/\Delta}$ females compared to *Smc3*$^{fl/fl}$, similar to the observations in zygotes derived from mature *Smc3*$^{\Delta/\Delta}$ females. Our findings suggest that zygotes from wild type juvenile females have persistent DNA lesions compared to zygotes from mature females, complicating the interpretation of the results. However, juvenile-derived mutant oocytes appear to contain sufficient SMC3 to partially prevent persistent DNA damage and enable the first mitotic division in *Smc3*$^{\Delta/\Delta}$ zygotes. Importantly, once ZGA occurs, *Smc3* provided from the paternal genome appears to be sufficient for developmental competence, once the first zygotic division is successfully completed.

Deletion of maternal *Smc3* in oocytes from mature females results in loss of cohesion and sister chromatid separation in zygotes arrested in metaphase (**Figure 4F**). We asked whether cohesion was intact in zygotes from juvenile *Smc3*$^{\Delta/\Delta}$ female mice. By analysis of spindles and centromeres from metaphase arrested juvenile-derived

Development • Accepted manuscript

Smc3$^{\Delta/\Delta}$ zygotes. Remarkably, chromosomes appeared stretched on the spindle, but the precocious separation of entire sister chromatids did not occur (**Figure 7A**). The length/width (L/W) ratio of the metaphase plate in juvenile-derived *Smc3*$^{\Delta/\Delta}$ zygotes was comparable to *Smc3*$^{fl/fl}$ zygotes **(Figure 7B)**, suggesting that unlike in adult-derived mutant zygotes, chromosomes were not completely stretched apart **(Figure 4C-D)**. Notably, we observed a Y-shaped chromatid structure in spindles from juvenile-derived *Smc3*$^{\Delta/\Delta}$ metaphase zygotes. We speculate that the Y structure is a consequence of losing centromeric cohesion on telocentric sister chromatids during proTAME arrest, consistent with the idea that prolonged arrest with intact microtubules may challenge centromeric cohesion. We also observed Y-shaped chromatids in chromosome spreads (**Figure S8**), indicating that intersister cohesion in the short p-arm of a telocentric chromosome is insufficient to withstand prolonged mitotic arrest. The stretched morphology of sister chromatids on the mitotic spindle of juvenile-derived mutant zygotes in proTAME (**Figure 7A**) is reminiscent of the stretched appearance of unperturbed adult-derived mutant zygotes in the live-cell imaging experiment (**Figure 4C**), suggesting the stretched appearance represents poor centromeric cohesion.

Interkinetochore distances increase with age in oocytes, indicative of a loss of centromeric cohesion (Duncan et al., 2012), but the physiological relevance is not understood. To further quantify centromeric cohesion, we measured interkinetochore distance in zygotes. Intensity profiles of sister kinetochore signals were traced by double Gaussian fitting to determine interkinetochore distances in metaphase (**Figure 7C**). We measured all distinguishable chromosome pairs with appropriate orientation in individual zygotes. In adult-derived *Smc3*$^{\Delta/\Delta}$ metaphase zygotes, we were unable to

Development • Accepted manuscript

quantify the interkinetochore distance since sister chromatid cohesion is completely lost and pairs are unidentifiable. In juvenile-derived *Smc3*$^{\Delta/\Delta}$ metaphase zygotes, the interkinetochore distance was significantly increased relative to *Smc3*$^{fl/fl}$ zygotes (**Figure 7C-D**). This strongly suggests that juvenile-derived *Smc3*$^{\Delta/\Delta}$ zygotes exhibit centromeric cohesion defects, but strikingly, can sustain developmental competence with cohesion in chromosome arms. By Western blot, however, we cannot detect significantly decreased levels of SMC3 in juvenile-derived *Smc3*$^{\Delta/\Delta}$ oocytes compared to the adult-derived *Smc3*$^{fl/fl}$ oocytes (**Figure S7A-B**). This imperfect correlation between the level of SMC3 and cohesion could be due to the insensitivity of Western blotting, and that protein levels on a Western blot are an imperfect indicator for SMC3 actively engaged in cohesion.

Loss of cohesion is associated with increased spindle length in yeast (Stephens et al., 2011), because there is less inward force constraining the elongation (Nannas et al., 2014), although this has not been examined in mouse zygotes. We measured the morphologies of sister chromatids and spindles in proTAME treated zygotes from both adult and juvenile females **(Figure 7E-F)**. The L/W ratio and length of the spindle in juvenile-derived *Smc3*$^{\Delta/\Delta}$ zygotes were significantly lower than in adult-derived *Smc3*$^{\Delta/\Delta}$ metaphase zygotes, suggesting that the metaphase plate and spindle morphologies improved and cohesion was more substantial **(Figure 7E-F)**. Moreover, the spindle length and length/width ratio of the spindle in the mutant were significantly higher than in juvenile-derived wild type zygotes, consistent with the loss of centromeric cohesion. In sum, the improved spindle length, chromosome morphology, and double-strand break repair in the juvenile-derived mutant zygotes are consistent with more cohesion

Development • Accepted manuscript

than in the adult-derived mutant zygotes. Overall, we conclude that sufficient maternal SMC3 in the *Smc3*$^{\Delta/\Delta}$ juvenile-derived oocytes exists to support chromosome integrity that enables developmental competence.

DISCUSSION

Here we demonstrate that *Smc3* is a maternal effect gene and sufficient levels of protein must be present in the oocyte for developmental competence. *Smc3* joins the sixty or so maternal effect genes that block progression from the 2-cell stage (Condic, 2016). SMC3 supports the fundamental processes of chromosome duplication and segregation, distinct from the cohesin subunit RAD21 and the cohesin binding partner CTCF, which are documented to support gene expression and imprinting (Ladstätter and Tachibana-Konwalski, 2016, Fedoriw et al., 2004, Wan et al., 2008). We demonstrate that maternal SMC3 is required to repair spontaneous DNA lesions following DNA replication in zygotes and to support accurate chromosome segregation during the first mitotic division post-fertilization to prevent aneuploidy. Despite the high rates of aneuploidy observed in early embryos in other studies that suggest aneuploidy is tolerated, our results suggest that the integrity and transmission of the zygotic genome is essential for successful embryogenesis and relies on proteins stored into the oocyte. Furthermore, we speculate that our findings are relevant to in vitro fertilization, in which preimplantation development is often monitored, because our results suggest elongated spindles in the zygote and micronuclei at the 2-cell stage serve as visual indicators of chromosomal instability correlating with poor outcomes.

Development • Accepted manuscript

Depletion of SMC3 in oocytes results in a unique phenotype relative to all other cohesin subunits that have been studied. REC8 and SMC1β null mutations are sterile due to meiotic failure, whereas *Smc1β*$^{fl/fl}$*;Gdf9-iCre* female mice are fertile, contrasting to the infertility observed in our breeding trials (Xu et al., 2005, Revenkova et al., 2004, Revenkova et al., 2010, Bannister et al., 2004) . Elimination of meiotic cohesin genes via *Gdf9-iCre* or *Zp3-Cre* drivers may not affect meiotic competence since sufficient protein remains. Since the zygote starts utilizing mitotic cohesin subunits after fertilization instead of meiotic subunits, elimination of meiotic cohesin may not affect developmental competence. On the other hand, elimination of RAD21 in oocytes via *Zp3-Cre* impacts developmental competence via paternal reprogramming and severely compromises entry into mitosis (Ladstätter and Tachibana-Konwalski, 2016). Unlike SMC3, which can be recycled, RAD21 is cleaved and destroyed after each cell division. We speculate that recycling of SMC3 allows cohesin-dependent repair of reprogramming-derived DNA lesions during G1. Alternatively, RAD21 may be uniquely involved in this repair. The first phenotype detected in *Smc3*$^{\Delta/\Delta}$ zygotes is persistent DNA lesions in G2. However, zygotes efficiently enter mitosis, and then the majority arrest at a 2-cell embryo. We failed to detect canonical ATR and ATM checkpoints in the 2-cell blocked *Smc3*$^{\Delta/\Delta}$ embryos. Determining the checkpoint mechanism will require further experimentation, but our findings suggest persistence of DNA damage and loss of cohesion in the zygote do not prompt a checkpoint arrest.

While many maternal effect genes point to the vital role of reprogramming and embryonic genome activation, our study suggests a critical role for chromosome maintenance and euploidy at the 2-cell stage, despite many studies demonstrating

Development • Accepted manuscript

frequent aneuploidy in early embryos. Studies of repair of spontaneous DNA damage from DNA replication and sister chromatid cohesion in a single cell cycle have mainly been carried out in mammalian cultured cells and yeast. Zygotes are an elegant model since factors can be depleted in the oocyte prior to the first mitotic division, plus zygotes reveal vital functions required in early embryos. 50 DSBs are estimated to occur during a normal S phase in a human cell (Vilenchik and Knudson, 2003). Our study is consistent with the proposal that cohesin is required to support their repair (Singh et al., 2020, Mondal et al., 2019, Ström and Sjögren, 2005), including replication fork restart (Frattini et al., 2017). Persistence of spontaneous DNA lesions in mutant zygotes is followed by sister chromatid mis-segregation. Lagging chromosomes and their subsequent incorporation into micronuclei could result from merotelic kinetochore attachment as well as compromised DNA replication, resulting in tangled chromosomes that lag in segregation and resolve into micronuclei (**Figure 8**), generating aneuploidies that are incompatible with developmental progression. *Filia* and *Bcas2* are other maternal effect genes required to maintain genomic integrity during cleavage stage mouse embryogenesis, supporting the proposal that euploidy can be a prerequisite for developmental competence (Zheng and Dean, 2009, Xu et al., 2015). A recent study found that aneuploidy from 2-cell embryos does not propagate into further developmental stages (Pauerova et al., 2020), consistent with our proposal that the mutant embryos arrest at the 2-cell stage due to mitosis-derived aneuploidy, although we cannot rule out faulty ZGA.

Centromeric cohesion is considered essential for accurate sister chromatid biorientation and segregation. Our study is consistent with previous studies that loss of

Development • Accepted manuscript

centromeric cohesion affects the physical architecture of the spindle, resulting in an elongated spindle (Stephens et al., 2011, Deehan Kenney and Heald, 2006). In a surprising twist, the Y-shaped chromatid structure in chromosome spreads derived from juvenile *Smc3*$^{\Delta/\Delta}$ zygotes, coupled with their ability to progress to the blastocyst stage, suggests that loss of centromeric cohesion can be compatible with successful mitosis and developmental competence. We speculate that the Y-shaped chromatid indicates that cohesion is completely lost surrounding the centromere and throughout the short arm of telocentric chromosomes. Cohesion in the q-arm of sister chromatids in the zygote is then sufficient to enable successful biorientation, mitotic division and subsequent embryogenesis. This observation is paradoxical in light of models based on cultured mammalian cells in which arm cohesion is removed by the prophase pathway and does not contribute to sister chromatid biorientation and segregation (Waizenegger et al., 2000, Sumara et al., 2002, Losada et al., 2002, Warren et al., 2000). Future efforts will be needed to ascertain how and where cohesion is needed for sister chromatid biorientation and segregation in early embryos.

Although the exact mechanism remains unclear, cohesin is a participant in homologous recombination (Litwin et al., 2018). Lack of cohesin or its loader leads to the accumulation of DNA lesions after γ-irradiation (Ferreira and Cooper, 2004, Sjögren and Nasmyth, 2001, Ström et al., 2007, Ström et al., 2004). However, our RAD51 analysis indicates that depletion of SMC3 does not disable the recruitment of homologous recombination proteins, consistent with a previous study in human cultured cells (Kong et al., 2014). Cohesin loads surrounding induced DSBs and holds sister chromatids together to facilitate their repair (Litwin et al., 2018, Watrin and Peters,

Development • Accepted manuscript

2006). We speculate that cohesion is established during DNA replication at sites of spontaneous damage, and that these normally invisible repair events contribute to the establishment of sister chromatid cohesion during S phase. In this speculative model, first postulated in budding yeast (Ström and Sjögren, 2005). spontaneous DNA damage during DNA replication from stalled forks results in the recruitment of cohesin to support sister chromatid repair. This cohesion then persists and contributes to sister chromatid cohesion for chromosome biorientation during mitosis. More work will be required to test this working model.

We demonstrate that genetically identical zygotes can differ in developmental competence depending on the age of mother. Although SMC3 protein is considered stable in aging oocytes (Tsutsumi et al., 2014), whether a natural age-associated decline in other cohesin subunits in the oocyte could impact developmental competence is an open question. Our study indicates that fertility is dramatically affected in mutant females in the span of ~2 weeks, as they progress from juvenile to adult. Distinct from studies that demonstrate aging related cohesion failures in meiosis and infertility (Tsutsumi et al., 2014, Lister et al., 2010, Chiang et al., 2010, Tachibana-Konwalski et al., 2010, Duncan et al., 2012, Hodges et al., 2005, Subramanian and Bickel, 2008, Murdoch et al., 2013), our study suggests that mutant juvenile females achieve developmental competence via higher dosage in oocytes that benefits zygotes. However, the juvenile stage is also associated with increased DNA lesions and altered spindle morphology in zygotes, even from wild type females. Oocyte quality declines with age, but pre-pubertal females also have poor quality oocytes (Karavani et al., 2019, Oktay et al., 2021). In the future careful consideration should be accorded to maternal

Development • Accepted manuscript

age when assessing maternal effect genes since we would have concluded that *Smc3* is not a maternal effect gene if we had only analyzed zygotes from juveniles, a protocol recommended by some textbooks (Behringer et al., 2014, Luo et al., 2011). Future efforts will benefit from additional depletion strategies, analysis at multiple ages, visualizing cohesin on chromosomes to better appreciate the functional pool, and analysis of additional proteins involved in developmental competence, chromosome segregation and spindle function (Ma et al., 2013, De and Kline, 2013).

In conclusion, our study provides novel insight into the working mechanism of maternal *Smc3* in early embryonic development. Oocyte-stored SMC3 is required to support the integrity of the zygotic genome during the very first round of DNA replication and sister chromatid segregation to successfully pass through the first and second mitotic divisions in the embryo. Our findings are broadly consistent with the recent proposal that meiosis-derived aneuploidy persists into embryogenesis, but mitosis-derived aneuploidy triggers arrest (Wartosch et al., 2021). Furthermore, our results suggest elongated spindles in zygotes and micronuclei in the 2-cell embryo are visual markers of poor developmental outcomes, which could be useful for IVF.

ACKNOWLEDGEMENTS

We are thankful to Ross Levine's lab for sharing the *Smc3* floxed mouse line. We thank Katja Wassmann and Elvira Nikalayevich (Institut de Biologie Paris Seine (IBPS), Sorbonne Universités, Centre National de la Recherche Scientifique UMR7622, Paris, France) for kind suggestions and tips for the SIR-DNA staining and live-cell imaging in

Development • Accepted manuscript

mouse zygotes. We are grateful to Heidi Monnin, Timothy Corbin and the Lab Animal Service Facility of the Stowers Institute for Medical Research (SIMR) for mouse husbandry and microinjection. We are grateful for helpful comments and suggestions from WT Yueh's thesis committee members Robb Krumlauf (SIMR), Jay Unruh (SIMR), and John Marko (Northwestern University). We sincerely thank Tamara Potapova (Gerton lab) and Francesca Duncan (Northwestern University) for helpful discussions and support.

AUTHOR CONTRIBUTIONS

W.Y. and J.L.G. conceived the study, designed the experiments, and wrote the manuscript. V.P.S performed the LacZ reporter assay and provided suggestions for the study design. W.Y. performed all the other experiments and analyzed all the data.

DECLARATION OF INTEREST

The authors declare no competing interest.

MATERIAL AND METHODS

Generation of Mouse Lines

All mice experimental protocols were approved by the Institutional Animal Care and Use Committee of the Stowers Institute for Medical Research (Kansas City, MO)

Development • Accepted manuscript

and were performed accordingly. Mice were housed in a barrier facility with constant temperature, humidity, and light at SIMR.

Mice were genotyped as described previously (de Vries et al., 2000, Lewandoski et al., 1997, Viny et al., 2015, Lan et al., 2004). *Smc3* heterozygous mice (*Smc3*$^{fl/+}$) were maintained in the C57BL/6J genetic background (Viny et al., 2015). *Smc3*$^{fl/fl}$*;Zp3-Cre* and *Smc3*$^{fl/fl}$*;Gdf9-iCre* male mice were generated by crossing *Smc3*$^{fl/+}$ females with Tg(*Zp3-Cre*) (JAX #003651) or Tg(*Gdf9-iCre*) males (JAX #011062) in the C57BL/6J genetic background. Experimental mice were generated from heterozygous or homozygous floxed females with homozygous floxed males positive for *Zp3-Cre* or *Gdf9-iCre*.

Breeding Trials

Fertility tests were carried out by crossing experimental females (6-8-week-old) with wild type C57BL/6J males. Female mice were checked for plugs every morning and each litter was recorded. Females were mated continuously for at least 6 months. The number of pups on the first day after parturition was counted as the litter size.

LacZ Reporter Assay

Male *Gdf9-iCre* mice were crossed with female *Gt(ROSA)26Sor*$^{tm1(LacZ)Cos}$ mice (R26R, JAX #003474) and embryos were collected in PBS at 13.5 dpc. Gonads were dissected from each embryo and fixed at 4˚C in fixative [1% formaldehyde, 0.2%

Development • Accepted manuscript

glutaraldehyde, 2 mM MgCl2, 5 mM EGTA, in wash solution (0.02% NP40 in PBS)] for 10 minutes. Gonads were washed three times for 15 minutes each, in wash solution at room temperature. After washing, gonads were put in staining solution (5 mM K3Fe(CN)6, 5 mM K4Fe(CN)6.3H2), 2 mM MgCl2, 0.01% Sodium deoxycholate, 0.02% NP40 and 1 mg/ml X-gal) overnight and the next morning embryos were washed, imaged and stored in fixative at 4˚C. Images were recorded using a Zeiss Axiovert microscope.

Histological analysis of ovaries and follicle counting

Histological tissue sections of the whole ovaries were prepared as previously described (Singh et al., 2019). In brief, whole ovaries were fixed in Modified Davidsons fixative for 6 hours at room temperature and overnight at 4˚C. The ovary was dehydrated, embedded in paraffin blocks, and then serial sectioned at 5 µm thickness. The slides were stained by hematoxylin and eosin (H&E). Images were acquired by a VS120 Slide Scanner (Olympus) with a 40x objective. Primordial, primary, secondary, and antral follicles were scored in every 5 sections throughout the entire ovary as previously described (Bristol-Gould et al., 2006, Duncan et al., 2017).

In vitro Maturation

To obtain fully grown germinal vesicle (GV) stage oocytes, 6-8-week-old females were injected with 5 IU PMSG. Prophase I arrested GV stage oocytes were isolated by physical dissection of ovaries in M2 medium with 5 µM milrinone. Isolated GV stage

Development • Accepted manuscript

oocytes were released from prophase I by briefly washing in L-15 medium (Thermo Fisher Scientific LLC # 11415-064). Oocytes were incubated in 90 µL drops of M16 medium covered with mineral oil at 37°C and 5% CO_2. Metaphase II oocytes were obtained 14 hours after incubation.

In vitro Culturing

To obtain zygotes, timed mating was performed by consecutive intraperitoneal injection of 5 IU PMSG followed by injection of 5 IU hCG 46-hours later. Super-ovulated female mice were crossed with C57BL/6J male mice after hCG injection. The referenced time point was defined by hCG injection for all related experiments (hour post-injection, hpi). Females were sacrificed 20 hpi and oviducts were isolated by surgical dissection and placed in M2 medium (#MR-015-D, Sigma). Zygotes were released from cumulus cells by a brief incubation with 500 µg/ µL hyaluronidase/M2 medium (H4272, Sigma). Fertilized zygotes were selected based on visible pronuclei. Unfertilized oocytes were discarded, and only fertilized zygotes were incubated in ~90 µL drops of KSOM medium (#MR-101-D, Sigma) at 37°C with 5% CO_2.

Microinjection

To increase the yield of zygotes, superovulation was performed by injection of 7.5IU CARD HyperOva (KYD-010-EX, Cosmo Bio USA) followed by injection of 7.5IU hCG 46 hours later. Zygotes were then isolated and incubated *in vitro*. The *Smc3* template was amplified from the Mouse SMC3 cDNA Clone in Cloning Vector

Development • Accepted manuscript

(ABIN4098669, Genomics-online) by PCR using Q5 High-Fidelity DNA Polymerase (#M0515, New England Biolabs), T3, and T7 primer pairs. mRNA was transcribed *in vitro* followed by 3' tailing by ultra T7 mMessage mMachine kit (AM1344, Invitrogen) under manufacturer's instructions. The purified mRNA was resuspended in either DEPC-treated water or TE buffer (10 mM Tris-HCl, 1 mM EDTA, pH=7.4) and then diluted to 10ng/μL in TE buffer prior to microinjection of 1-2 picoliters (pL).

Fixation and Immunofluorescence

To properly identify the cell cycle phase, zygotes were pulsed with 100 mM EdU for 30 min. G1, S, and G2 phase zygotes were classified by both the timing of fixation (G1: 20.5-22.5 hpi, S: 24-26 hpi, G2: 26-28 hpi) and the presence of EdU incorporation in the pronucleus. Only S phase zygotes incorporated EdU into the pronucleus. Any zygote collected from the G1 or G2 phase time points with EdU signal was disqualified as a G1 or G2 phase pronucleus. To verify global RNA transcription, zygotes were pulsed with 1 mM 5-EU for 2 hours before fixation.

To examine checkpoint activation, 2-cell stage embryos were collected at 53.5 hpi (~10% of wild type embryos reached the 4-cell stage at this timepoint). To introduce replication stress and exogenous DNA damage, zygotes were cultured with 4mM hydroxyurea at 24 hpi for 4 hours before fixation.

Metaphase zygotes were obtained from incubation with 10 μM ProTAME (I-440, BostonBiochem, MA) to inhibit the Anaphase-promoting complex (APC) for 3-4 hours. Oocytes and zygotes were fixed with 2% paraformaldehyde (PFA)/PBS for one hour at

Development • Accepted manuscript

room temperature. Fixed samples were washed twice with blocking solution (0.3% BSA, 1X PBS, 0.01% tween-20, 0.02% sodium azide (NaN_3)) for 5 minutes and then stored at 4°C. Samples were incubated in a permeabilization solution (0.3% BSA, 1X PBS, 0.1% Triton X-100, 0.02% NaN_3) for 20 min and then washed twice with blocking solution for 5 min. Samples pulsed with EdU or 5EU were processed following the guidelines of the Click-iT EdU Alexa Fluor 488 or 647 imaging kit (Invitrogen) as needed. Samples were immediately washed with blocking solution for 3 times for 5 min each. α-tubulin 488 Alexa Fluor conjugate (#16-232, Sigma) (1:200), rabbit α-γH2A.X (#9718, Cell Signaling) (1:500), mouse α-γH2A.X (#05-636, Sigma) (1:500), RPA70 (#PA5-21976, Life Technologies) (1:100), RAD51 (#PC130, Sigma) (1:250), centromere serum (#HCT-0100, ImmunoVision, AR, USA) (1:100), Chk1 (#2360, Cell signaling) (1:100), and p-ATM (#39530, Active Motif) (1:100) primary antibodies were diluted in blocking solution and incubated overnight at 4°C. The next day primary antibodies were washed out with blocking solution for 10 min 5 times and incubated in Alexa Fluor 647 α-human (A-21445, Thermo Fisher Scientific LLC), Alexa Fluor 647 α-mouse (A31571, Life Technologies), Alexa Fluor 594 α-rabbit (A-11072, Thermo Fisher Scientific LLC), Alexa Flour 594 α-mouse (A-11020, Thermo Fisher Scientific LLC), or Alexa Fluor 488 α-mouse secondary antibodies (A-28175, Thermo Fisher Scientific LLC) diluted in blocking solution for 2 hours at room temperature. Secondary antibodies were washed out with blocking solution for 10 min 5 times. Samples were mounted on glass slides in VECTASHIELD Antifade Mounting Medium with DAPI (#H-1200-10, Vector Laboratories, USA). Image acquisition was performed on a Carl Zeiss LSM-710 confocal microscope with a 63x oil immersion objective and Z-stacks were taken every 0.5 µm.

Development • Accepted manuscript

Chromosome Spreads

Slides of chromosome spreads were prepared as described before (Hodges and Hunt, 2002). In brief, zona pellucida was removed in acidic M2 medium. Oocytes in metaphase II or zygotes in metaphase were briefly washed with M2 medium and then deposited on a glass slide with ~70µL drops of spread solution (1% PFA, 0.15% Triton X-100, 3mM dithiothreitol in distilled H_2O (pH 9.5)). Slides were incubated in a humid chamber for 1 hour and then dried overnight. Slides could be stored at -20°C before staining. Debris was washed from slides using 0.4% Kodak Photo-Flo 200 solution for 5 min twice, 1X PBS for 5 min, and 1X PBST (0.1%). Slides were incubated in the blocking solution for 1 hour. Subsequent immunofluorescence was performed as mentioned earlier and an Alexa Fluor 488 α-human secondary antibody was used (A-11013, Thermo Fisher Scientific LLC).

Live-cell imaging Microscopy

Live zygotes were incubated with 100 nM SIR-DNA dye (#CY-SC007, Cytoskeleton, Denver) diluted in ~90 µL KSOM medium for 30 min. Stained embryos were then transferred to an Interchangeable Coverglass Dish (#190310-35, Bioptechs, PA, USA) with 30mm diameter, #1.5 thickness coverslip (#30-1313-0319, Bioptechs, PA, USA) in SIR-DNA/KSOM medium. Image acquisition was performed on a Nikon 3PO spinning disc microscope with a 40x water objective. Microscopy was controlled by Nikon's Confocal NIS-Elements Package. Time-lapse images were acquired with ~13 z-sections of 3 µm every 3 min.

Development • Accepted manuscript

Western Blot Analysis

Fully grown GV stage oocytes for each group were isolated as mentioned earlier, and briefly washed with L-15 medium. 30 oocytes per tube were collected in 10 µL of L15-medium and then snap-frozen in liquid nitrogen. Frozen oocytes were stored at -80°C before testing. Proteins were extracted using Bio-Rad sample buffer (#161-0747, Bio-Rad) with 2-Mercaptoethanol (M7522, Sigma) at 95°C for 10 min, centrifuged at 12000 rpm for 2 min, and the supernatant was collected. Proteins were separated using Bio-Rad 4-15% gradient gels (#456-1084, Bio-Rad) and blotted on PVDF membrane (#10061-494, GE Healthcare). Blots were blocked with 0.3% ECL Prime Blocking Reagent (RPN418, GE Healthcare) in Tris-buffered saline supplemented with 0.01% Tween (TBSTw) for 1 hour. SMC3 (#ab9263, Abcam) (1:2000) and γ-tubulin (#ab11316) (1:1000) primary antibodies were diluted in 0.3% blocking buffer at 4°C overnight. Blots were washed by TBSTw for 10 min three times and then incubated with α-rabbit or α-mouse HRP-conjugated secondary antibodies (NA931V and NA934V, GE Healthcare) (1:5000). Blots were washed by TBSTw for 10 min three times and then developed by ECL Prime Western Blotting Detection Reagent kit (RPN2232, Ge Healthcare).

Quantification, Foci Counting, and Imaging Analysis

Image analysis was performed using open-source Fiji software (Schindelin et al., 2012). The intensities of the Western blots were quantified using the gel analysis method outlined in ImageJ. Foci quantification was performed in as described previously with minor modifications (Cai et al., 2009). Briefly, image stacks were

Development • Accepted manuscript

background-subtracted by the rolling radius of 1.32 µm or 3.86 µm, and foci counting was performed by analysis of particles > 0.5 μm^2 or > 0.01 μm^2 corresponding to the cell size covered by the entire Z-stack range. Thresholds were kept (20, 255) and (150, 255) within all experiments.

To quantify the L/D ratio of metaphase plate and spindle, the Z-projections of stack images were Gaussian blurred by the radius of 1.37 µm in the live-cell imaging and 1.5 µm in the immunostaining of metaphase zygotes. Thresholds were automated within all experiments to visualize the boundaries for length measurement.

The quantification of inter-kinetochore distance was performed as previous described (Cahoon et al., 2017). In brief, only image stacks with appropriate orientation were selected for the quantification. All distinguishable centromere pairs were counted in each xy image. The line profile of CREST signal along x axis were generated from aligning the center of two peaks. The average profiles were fit into a two gaussian model to determine the width of two peaks.

Statistics

Statistical parameters and tests are described in the figure legends. Statistical analysis was done using Microsoft Excel 365 and R studio. The parametric two-tail unpaired t-test was performed for datasets, while the nonparametric unpaired Mann-Whitney test was used for datasets not passing the Iglewicz and Hoaglin's robust test for multiple outliers within the z score of 3.5. Fisher's exact test was performed to examine the contingency table datasets.

Development • Accepted manuscript

REFERENCES

AOKI, F., WORRAD, D. M. & SCHULTZ, R. M. 1997. Regulation of Transcriptional Activity during the First and Second Cell Cycles in the Preimplantation Mouse Embryo. *Developmental Biology,* 181**,** 296-307.

ARAGÓN, L. 2018. The Smc5/6 Complex: New and Old Functions of the Enigmatic Long-Distance Relative. *Annual Review of Genetics,* 52**,** 89-107.

ARNAUDEAU, C., LUNDIN, C. & HELLEDAY, T. 2001. DNA double-strand breaks associated with replication forks are predominantly repaired by homologous recombination involving an exchange mechanism in mammalian cells11Edited by J. Karn. *Journal of Molecular Biology,* 307**,** 1235-1245.

BANNISTER, L. A., REINHOLDT, L. G., MUNROE, R. J. & SCHIMENTI, J. C. 2004. Positional cloning and characterization of mouse mei8, a disrupted allelle of the meiotic cohesin Rec8. *Genesis,* 40**,** 184-94.

BECKOUËT, F., HU, B., ROIG, M. B., SUTANI, T., KOMATA, M., ULUOCAK, P., KATIS, V. L., SHIRAHIGE, K. & NASMYTH, K. 2010. An Smc3 Acetylation Cycle Is Essential for Establishment of Sister Chromatid Cohesion. *Molecular Cell,* 39**,** 689-699.

BEHRINGER, R., GERTSENSTEIN, M., NAGY, K. V. & NAGY, A. 2014. *Manipulating the mouse embryo : a laboratory manual,* Cold Spring Harbor, New York, Cold Spring Harbor Laboratory Press.

BORGES, V., LEHANE, C., LOPEZ-SERRA, L., FLYNN, H., SKEHEL, M., BEN-SHAHAR, T. R. & UHLMANN, F. 2010. Hos1 Deacetylates Smc3 to Close the Cohesin Acetylation Cycle. *Molecular Cell,* 39**,** 677-688.

BRISTOL-GOULD, S. K., KREEGER, P. K., SELKIRK, C. G., KILEN, S. M., COOK, R. W., KIPP, J. L., SHEA, L. D., MAYO, K. E. & WOODRUFF, T. K. 2006. Postnatal regulation of germ cells by activin: The establishment of the initial follicle pool. *Developmental Biology,* 298**,** 132-148.

BURKHARDT, S., BORSOS, M., SZYDLOWSKA, A., GODWIN, J., WILLIAMS, SUZANNAH A., COHEN, PAULA E., HIROTA, T., SAITOU, M. & TACHIBANA-KONWALSKI, K. 2016. Chromosome Cohesion Established by Rec8-Cohesin in Fetal Oocytes Is Maintained without Detectable Turnover in Oocytes Arrested for Months in Mice. *Current Biology,* 26**,** 678-685.

CAHOON, C. K., YU, Z., WANG, Y., GUO, F., UNRUH, J. R., SLAUGHTER, B. D. & HAWLEY, R. S. 2017. Superresolution expansion microscopy reveals the three-dimensional organization of the *Drosophila* synaptonemal complex. *Proceedings of the National Academy of Sciences,* 114**,** E6857.

CAI, Z., VALLIS, K. A. & REILLY, R. M. 2009. Computational analysis of the number, area and density of γ-H2AX foci in breast cancer cells exposed to 111In-DTPA-hEGF or γ-rays using Image-J software. *International Journal of Radiation Biology,* 85**,** 262-271.

CHIANG, T., DUNCAN, F. E., SCHINDLER, K., SCHULTZ, R. M. & LAMPSON, M. A. 2010. Evidence that Weakened Centromere Cohesion Is a Leading Cause of Age-Related Aneuploidy in Oocytes. *Current Biology,* 20**,** 1522-1528.

CONDIC, M. L. 2016. The Role of Maternal-Effect Genes in Mammalian Development: Are Mammalian Embryos Really an Exception? *Stem Cell Reviews and Reports,* 12**,** 276-284.

CONN, C. W., LEWELLYN, A. L. & MALLER, J. L. 2004. The DNA Damage Checkpoint in Embryonic Cell Cycles Is Dependent on the DNA-to-Cytoplasmic Ratio. *Developmental Cell,* 7**,** 275-281.

DE, S. & KLINE, D. 2013. Evidence for the requirement of 14-3-3eta (YWHAH) in meiotic spindle assembly during mouse oocyte maturation. *BMC Developmental Biology,* 13**,** 10.

Development • Accepted manuscript

DE VRIES, W. N., BINNS, L. T., FANCHER, K. S., DEAN, J., MOORE, R., KEMLER, R. & KNOWLES, B. B. 2000. Expression of Cre recombinase in mouse oocytes: a means to study maternal effect genes. *Genesis,* 26**,** 110-2.

DEARDORFF, M. A., BANDO, M., NAKATO, R., WATRIN, E., ITOH, T., MINAMINO, M., SAITOH, K., KOMATA, M., KATOU, Y., CLARK, D., COLE, K. E., DE BAERE, E., DECROOS, C., DI DONATO, N., ERNST, S., FRANCEY, L. J., GYFTODIMOU, Y., HIRASHIMA, K., HULLINGS, M., ISHIKAWA, Y., JAULIN, C., KAUR, M., KIYONO, T., LOMBARDI, P. M., MAGNAGHI-JAULIN, L., MORTIER, G. R., NOZAKI, N., PETERSEN, M. B., SEIMIYA, H., SIU, V. M., SUZUKI, Y., TAKAGAKI, K., WILDE, J. J., WILLEMS, P. J., PRIGENT, C., GILLESSEN-KAESBACH, G., CHRISTIANSON, D. W., KAISER, F. J., JACKSON, L. G., HIROTA, T., KRANTZ, I. D. & SHIRAHIGE, K. 2012. HDAC8 mutations in Cornelia de Lange syndrome affect the cohesin acetylation cycle. *Nature,* 489**,** 313-317.

DEEHAN KENNEY, R. & HEALD, R. 2006. Essential roles for cohesin in kinetochore and spindle function in *Xenopus* egg extracts. *Journal of Cell Science,* 119**,** 5057.

DUNCAN, F. E., HORNICK, J. E., LAMPSON, M. A., SCHULTZ, R. M., SHEA, L. D. & WOODRUFF, T. K. 2012. Chromosome cohesion decreases in human eggs with advanced maternal age. *Aging cell,* 11**,** 1121-1124.

DUNCAN, F. E., JASTI, S., PAULSON, A., KELSH, J. M., FEGLEY, B. & GERTON, J. L. 2017. Age-associated dysregulation of protein metabolism in the mammalian oocyte. *Aging Cell,* 16**,** 1381-1393.

FEDORIW, A. M., STEIN, P., SVOBODA, P., SCHULTZ, R. M. & BARTOLOMEI, M. S. 2004. Transgenic RNAi Reveals Essential Function for CTCF in *H19* Gene Imprinting. *Science,* 303**,** 238.

FERREIRA, M. G. & COOPER, J. P. 2004. Two modes of DNA double-strand break repair are reciprocally regulated through the fission yeast cell cycle. *Genes & development,* 18**,** 2249-2254.

FRATTINI, C., VILLA-HERNÁNDEZ, S., PELLICANÒ, G., JOSSEN, R., KATOU, Y., SHIRAHIGE, K. & BERMEJO, R. 2017. Cohesin Ubiquitylation and Mobilization Facilitate Stalled Replication Fork Dynamics. *Molecular Cell,* 68**,** 758-772.e4.

HAARHUIS, JUDITH H. I., ELBATSH, AHMED M. O., VAN DEN BROEK, B., CAMPS, D., ERKAN, H., JALINK, K., MEDEMA, RENÉ H. & ROWLAND, BENJAMIN D. 2013. WAPL-Mediated Removal of Cohesin Protects against Segregation Errors and Aneuploidy. *Current Biology,* 23**,** 2071-2077.

HAMATANI, T., CARTER, M. G., SHAROV, A. A. & KO, M. S. 2004. Dynamics of global gene expression changes during mouse preimplantation development. *Dev Cell,* 6**,** 117-31.

HASSOLD, T. & HUNT, P. 2001. To err (meiotically) is human: the genesis of human aneuploidy. *Nature Reviews Genetics,* 2**,** 280-291.

HODGES, C. A. & HUNT, P. A. 2002. Simultaneous analysis of chromosomes and chromosome-associated proteins in mammalian oocytes and embryos. *Chromosoma,* 111**,** 165-9.

HODGES, C. A., REVENKOVA, E., JESSBERGER, R., HASSOLD, T. J. & HUNT, P. A. 2005. SMC1β-deficient female mice provide evidence that cohesins are a missing link in age-related nondisjunction. *Nature Genetics,* 37**,** 1351.

HUNT, P. 2017. Oocyte Biology: Do the Wheels Fall Off with Age? *Current Biology,* 27**,** R266-R269.

HWANG, G., SUN, F., BRIEN, M., EPPIG, J. J., HANDEL, M. A. & JORDAN, P. W. 2017. SMC5/6 is required for the formation of segregation-competent bivalent chromosomes during meiosis I in mouse oocytes. *Development,* 144**,** 1648.

JUKAM, D., SHARIATI, S. A. M. & SKOTHEIM, J. M. 2017. Zygotic Genome Activation in Vertebrates. *Developmental Cell,* 42**,** 316-332.

KARAVANI, G., SCHACHTER-SAFRAI, N., REVEL, A., MORDECHAI-DANIEL, T., BAUMAN, D. & IMBAR, T. 2019. In vitro maturation rates in young premenarche patients. *Fertility and Sterility,* 112**,** 315-322.

KATO, Y. & TSUNODA, Y. 1992. Synchronous division of mouse two-cell embryos with nocodazole in vitro. *J Reprod Fertil,* 95**,** 39-43.

Development • Accepted manuscript

KIM, K.-H. & LEE, K.-A. 2014. Maternal effect genes: Findings and effects on mouse embryo development. *Clin Exp Reprod Med,* 41**,** 47-61.

KONG, X., BALL, A. R., PHAM, H. X., ZENG, W., CHEN, H.-Y., SCHMIESING, J. A., KIM, J.-S., BERNS, M. & YOKOMORI, K. 2014. Distinct Functions of Human Cohesin-SA1 and Cohesin-SA2 in Double-Strand Break Repair. *Molecular and Cellular Biology,* 34**,** 685.

LADSTÄTTER, S. & TACHIBANA-KONWALSKI, K. 2016. A Surveillance Mechanism Ensures Repair of DNA Lesions during Zygotic Reprogramming. *Cell,* 167**,** 1774-1787.e13.

LAN, Z.-J., XU, X. & COONEY, A. J. 2004. Differential Oocyte-Specific Expression of Cre Recombinase Activity in GDF-9-iCre, Zp3cre, and Msx2Cre Transgenic Mice1. *Biology of Reproduction,* 71**,** 1469-1474.

LEWANDOSKI, M., WASSARMAN, K. M. & MARTIN, G. R. 1997. Zp3–cre, a transgenic mouse line for the activation or inactivation of loxP-flanked target genes specifically in the female germ line. *Current Biology,* 7**,** 148-151.

LISTER, L. M., KOUZNETSOVA, A., HYSLOP, L. A., KALLEAS, D., PACE, S. L., BAREL, J. C., NATHAN, A., FLOROS, V., ADELFALK, C., WATANABE, Y., JESSBERGER, R., KIRKWOOD, T. B., HÖÖG, C. & HERBERT, M. 2010. Age-related meiotic segregation errors in mammalian oocytes are preceded by depletion of cohesin and Sgo2. *Curr Biol,* 20**,** 1511-21.

LITWIN, I., PILARCZYK, E. & WYSOCKI, R. 2018. The Emerging Role of Cohesin in the DNA Damage Response. *Genes,* 9**,** 581.

LOSADA, A., HIRANO, M. & HIRANO, T. 1998. Identification of Xenopus SMC protein complexes required for sister chromatid cohesion. *Genes Dev,* 12**,** 1986-97.

LOSADA, A., HIRANO, M. & HIRANO, T. 2002. Cohesin release is required for sister chromatid resolution, but not for condensin-mediated compaction, at the onset of mitosis. *Genes & Development,* 16**,** 3004-3016.

LUK, B. H.-K. & LOKE, A. Y. 2015. The Impact of Infertility on the Psychological Well-Being, Marital Relationships, Sexual Relationships, and Quality of Life of Couples: A Systematic Review. *Journal of Sex & Marital Therapy,* 41**,** 610-625.

LUO, C., ZUÑIGA, J., EDISON, E., PALLA, S., DONG, W. & PARKER-THORNBURG, J. 2011. Superovulation strategies for 6 commonly used mouse strains. *Journal of the American Association for Laboratory Animal Science : JAALAS,* 50**,** 471-478.

MA, J. Y., LI, M., LUO, Y. B., SONG, S., TIAN, D., YANG, J., ZHANG, B., HOU, Y., SCHATTEN, H., LIU, Z. & SUN, Q. Y. 2013. Maternal factors required for oocyte developmental competence in mice: transcriptome analysis of non-surrounded nucleolus (NSN) and surrounded nucleolus (SN) oocytes. *Cell Cycle,* 12**,** 1928-38.

MEIER, M., GRANT, J., DOWDLE, A., THOMAS, A., GERTON, J., COLLAS, P., SULLIVAN, J. M. & HORSFIELD, J. A. 2018. Cohesin facilitates zygotic genome activation in zebrafish. *Development,* 145**,** dev156521.

MONDAL, G., STEVERS, M., GOODE, B., ASHWORTH, A. & SOLOMON, D. A. 2019. A requirement for STAG2 in replication fork progression creates a targetable synthetic lethality in cohesin-mutant cancers. *Nature Communications,* 10**,** 1686.

MURAYAMA, Y., SAMORA, C. P., KUROKAWA, Y., IWASAKI, H. & UHLMANN, F. 2018. Establishment of DNA-DNA Interactions by the Cohesin Ring. *Cell,* 172**,** 465-477.e15.

MURDOCH, B., OWEN, N., STEVENSE, M., SMITH, H., NAGAOKA, S., HASSOLD, T., MCKAY, M., XU, H., FU, J., REVENKOVA, E., JESSBERGER, R. & HUNT, P. 2013. Altered Cohesin Gene Dosage Affects Mammalian Meiotic Chromosome Structure and Behavior. *PLOS Genetics,* 9**,** e1003241.

NAMDAR, A., NAGHIZADEH, M. M., ZAMANI, M., YAGHMAEI, F. & SAMENI, M. H. 2017. Quality of life and general health of infertile women. *Health and quality of life outcomes,* 15**,** 139-139.

Development • Accepted manuscript

NANNAS, N. J., O'TOOLE, E. T., WINEY, M. & MURRAY, A. W. 2014. Chromosomal attachments set length and microtubule number in the Saccharomyces cerevisiae mitotic spindle. *Molecular Biology of the Cell,* 25**,** 4034-4048.

NASMYTH, K. & HAERING, C. H. 2005. THE STRUCTURE AND FUNCTION OF SMC AND KLEISIN COMPLEXES. *Annual Review of Biochemistry,* 74**,** 595-648.

OKTAY, K. H., MARIN, L., PETRIKOVSKY, B., TERRANI, M. & BABAYEV, S. N. 2021. Delaying Reproductive Aging by Ovarian Tissue Cryopreservation and Transplantation: Is it Prime Time? *Trends Mol Med*.

PAUEROVA, T., RADONOVA, L., KOVACOVICOVA, K., NOVAKOVA, L., SKULTETY, M. & ANGER, M. 2020. Aneuploidy during the onset of mouse embryo development. *Reproduction,* 160**,** 773-782.

RADONOVA, L., SVOBODOVA, T. & ANGER, M. 2019. Regulation of the cell cycle in early mammalian embryos and its clinical implications. *Int J Dev Biol,* 63**,** 113-122.

REVENKOVA, E., EIJPE, M., HEYTING, C., HODGES, C. A., HUNT, P. A., LIEBE, B., SCHERTHAN, H. & JESSBERGER, R. 2004. Cohesin SMC1β is required for meiotic chromosome dynamics, sister chromatid cohesion and DNA recombination. *Nature Cell Biology,* 6**,** 555-562.

REVENKOVA, E., HERRMANN, K., ADELFALK, C. & JESSBERGER, R. 2010. Oocyte cohesin expression restricted to predictyate stages provides full fertility and prevents aneuploidy. *Current biology : CB,* 20**,** 1529-1533.

SATISH KUMAR, A., MEGUMI, T., TSUTOMU, S., JUN, T., NORIO, U. & OHTSURA, N. 2007. Delayed and stage specific phosphorylation of H2AX during preimplantation development of γ-irradiated mouse embryos. *Reproduction,* 133**,** 415-422.

SCHINDELIN, J., ARGANDA-CARRERAS, I., FRISE, E., KAYNIG, V., LONGAIR, M., PIETZSCH, T., PREIBISCH, S., RUEDEN, C., SAALFELD, S., SCHMID, B., TINEVEZ, J.-Y., WHITE, D. J., HARTENSTEIN, V., ELICEIRI, K., TOMANCAK, P. & CARDONA, A. 2012. Fiji: an open-source platform for biological-image analysis. *Nature Methods,* 9**,** 676-682.

SCHULTZ, R. M. 1993. Regulation of zygotic gene activation in the mouse. *BioEssays,* 15**,** 531-538.

SCHULTZ, R. M. 2002. The molecular foundations of the maternal to zygotic transition in the preimplantation embryo. *Human Reproduction Update,* 8**,** 323-331.

SINGH, V. P., MCKINNEY, S. & GERTON, J. L. 2020. Persistent DNA Damage and Senescence in the Placenta Impacts Developmental Outcomes of Embryos. *Developmental Cell*.

SINGH, V. P., YUEH, W. T., GERTON, J. L. & DUNCAN, F. E. 2019. Oocyte-specific deletion of Hdac8 in mice reveals stage-specific effects on fertility. *Reproduction*.

SJÖGREN, C. & NASMYTH, K. 2001. Sister chromatid cohesion is required for postreplicative double-strand break repair in Saccharomyces cerevisiae. *Current Biology,* 11**,** 991-995.

SOTO, M., GARCÍA-SANTISTEBAN, I., KRENNING, L., MEDEMA, R. H. & RAAIJMAKERS, J. A. 2018. Chromosomes trapped in micronuclei are liable to segregation errors. *Journal of cell science,* 131**,** jcs214742.

STEPHENS, A. D., HAASE, J., VICCI, L., TAYLOR, R. M., II & BLOOM, K. 2011. Cohesin, condensin, and the intramolecular centromere loop together generate the mitotic chromatin spring. *Journal of Cell Biology,* 193**,** 1167-1180.

STRÖM, L., KARLSSON, C., LINDROOS, H. B., WEDAHL, S., KATOU, Y., SHIRAHIGE, K. & SJÖGREN, C. 2007. Postreplicative Formation of Cohesion Is Required for Repair and Induced by a Single DNA Break. *Science,* 317**,** 242.

STRÖM, L., LINDROOS, H. B., SHIRAHIGE, K. & SJÖGREN, C. 2004. Postreplicative Recruitment of Cohesin to Double-Strand Breaks Is Required for DNA Repair. *Molecular Cell,* 16**,** 1003-1015.

STRÖM, L. & SJÖGREN, C. 2005. DNA Damage-Induced Cohesion. *Cell Cycle,* 4**,** 536-539.

SUBRAMANIAN, V. V. & BICKEL, S. E. 2008. Aging predisposes oocytes to meiotic nondisjunction when the cohesin subunit SMC1 is reduced. *PLoS genetics,* 4**,** e1000263-e1000263.

Development • Accepted manuscript

SUMARA, I., VORLAUFER, E., STUKENBERG, P. T., KELM, O., REDEMANN, N., NIGG, E. A. & PETERS, J.-M. 2002. The Dissociation of Cohesin from Chromosomes in Prophase Is Regulated by Polo-like Kinase. *Molecular Cell,* 9**,** 515-525.

TACHIBANA-KONWALSKI, K., GODWIN, J., VAN DER WEYDEN, L., CHAMPION, L., KUDO, N. R., ADAMS, D. J. & NASMYTH, K. 2010. Rec8-containing cohesin maintains bivalents without turnover during the growing phase of mouse oocytes. *Genes & development,* 24**,** 2505-2516.

THADANI, R. & UHLMANN, F. 2015. Chromosome Condensation: Weaving an Untangled Web. *Current Biology,* 25**,** R663-R666.

THOMA, M. E., MCLAIN, A. C., LOUIS, J. F., KING, R. B., TRUMBLE, A. C., SUNDARAM, R. & BUCK LOUIS, G. M. 2013. Prevalence of infertility in the United States as estimated by the current duration approach and a traditional constructed approach. *Fertil Steril,* 99**,** 1324-1331.e1.

THOMPSON, S. L. & COMPTON, D. A. 2011. Chromosome missegregation in human cells arises through specific types of kinetochore–microtubule attachment errors. *Proceedings of the National Academy of Sciences,* 108**,** 17974.

TSUTSUMI, M., FUJIWARA, R., NISHIZAWA, H., ITO, M., KOGO, H., INAGAKI, H., OHYE, T., KATO, T., FUJII, T. & KURAHASHI, H. 2014. Age-Related Decrease of Meiotic Cohesins in Human Oocytes. *PLOS ONE,* 9**,** e96710.

UHLMANN, F. & NASMYTH, K. 1998. Cohesion between sister chromatids must be established during DNA replication. *Current Biology,* 8**,** 1095-1102.

VÁZQUEZ-DIEZ, C. & FITZHARRIS, G. 2018. Causes and consequences of chromosome segregation error in preimplantation embryos. *Reproduction,* 155**,** R63-R76.

VÁZQUEZ-DIEZ, C., PAIM, L. M. G. & FITZHARRIS, G. 2019. Cell-Size-Independent Spindle Checkpoint Failure Underlies Chromosome Segregation Error in Mouse Embryos. *Current Biology,* 29**,** 865-873.e3.

VILENCHIK, M. M. & KNUDSON, A. G. 2003. Endogenous DNA double-strand breaks: Production, fidelity of repair, and induction of cancer. *Proceedings of the National Academy of Sciences,* 100**,** 12871.

VINY, A. D., OTT, C. J., SPITZER, B., RIVAS, M., MEYDAN, C., PAPALEXI, E., YELIN, D., SHANK, K., REYES, J., CHIU, A., ROMIN, Y., BOYKO, V., THOTA, S., MACIEJEWSKI, J. P., MELNICK, A., BRADNER, J. E. & LEVINE, R. L. 2015. Dose-dependent role of the cohesin complex in normal and malignant hematopoiesis. *The Journal of experimental medicine,* 212**,** 1819-1832.

WAIZENEGGER, I. C., HAUF, S., MEINKE, A. & PETERS, J.-M. 2000. Two Distinct Pathways Remove Mammalian Cohesin from Chromosome Arms in Prophase and from Centromeres in Anaphase. *Cell,* 103**,** 399-410.

WAN, L.-B., PAN, H., HANNENHALLI, S., CHENG, Y., MA, J., FEDORIW, A., LOBANENKOV, V., LATHAM, K. E., SCHULTZ, R. M. & BARTOLOMEI, M. S. 2008. Maternal depletion of CTCF reveals multiple functions during oocyte and preimplantation embryo development. *Development,* 135**,** 2729-2738.

WARREN, W. D., STEFFENSEN, S., LIN, E., COELHO, P., LOUPART, M. L., COBBE, N., LEE, J. Y., MCKAY, M. J., ORR-WEAVER, T., HECK, M. M. S. & SUNKEL, C. E. 2000. The *Drosophila* RAD21 cohesin persists at the centromere region in mitosis. *Current Biology,* 10**,** 1463-1466.

WARTOSCH, L., SCHINDLER, K., SCHUH, M., GRUHN, J. R., HOFFMANN, E. R., MCCOY, R. C. & XING, J. 2021. Origins and mechanisms leading to aneuploidy in human eggs. *Prenatal Diagnosis,* 41**,** 620-630.

WATRIN, E. & PETERS, J.-M. 2006. Cohesin and DNA damage repair. *Experimental Cell Research,* 312**,** 2687-2693.

XIONG, B., LU, S. & GERTON, J. L. 2010. Hos1 Is a Lysine Deacetylase for the Smc3 Subunit of Cohesin. *Current Biology,* 20**,** 1660-1665.

Development • Accepted manuscript

XU, H., BEASLEY, M. D., WARREN, W. D., VAN DER HORST, G. T. J. & MCKAY, M. J. 2005. Absence of Mouse REC8 Cohesin Promotes Synapsis of Sister Chromatids in Meiosis. *Developmental Cell,* 8**,** 949-961.

XU, Q., WANG, F., XIANG, Y., ZHANG, X., ZHAO, Z.-A., GAO, Z., LIU, W., LU, X., LIU, Y., YU, X.-J., WANG, H., HUANG, J., YI, Z., GAO, S. & LI, L. 2015. Maternal BCAS2 protects genomic integrity in mouse early embryonic development. *Development,* 142**,** 3943-3953.

ZANONI, M., GARAGNA, S., REDI, C. A. & ZUCCOTTI, M. 2009. The 2-cell block occurring during development of outbred mouse embryos is rescued by cytoplasmic factors present in inbred metaphase II oocytes. *Int J Dev Biol,* 53**,** 129-34.

ZHENG, P. & DEAN, J. 2009. Role of *Filia*, a maternal effect gene, in maintaining euploidy during cleavage-stage mouse embryogenesis. *Proceedings of the National Academy of Sciences,* 106**,** 7473.

Development • Accepted manuscript

Figures

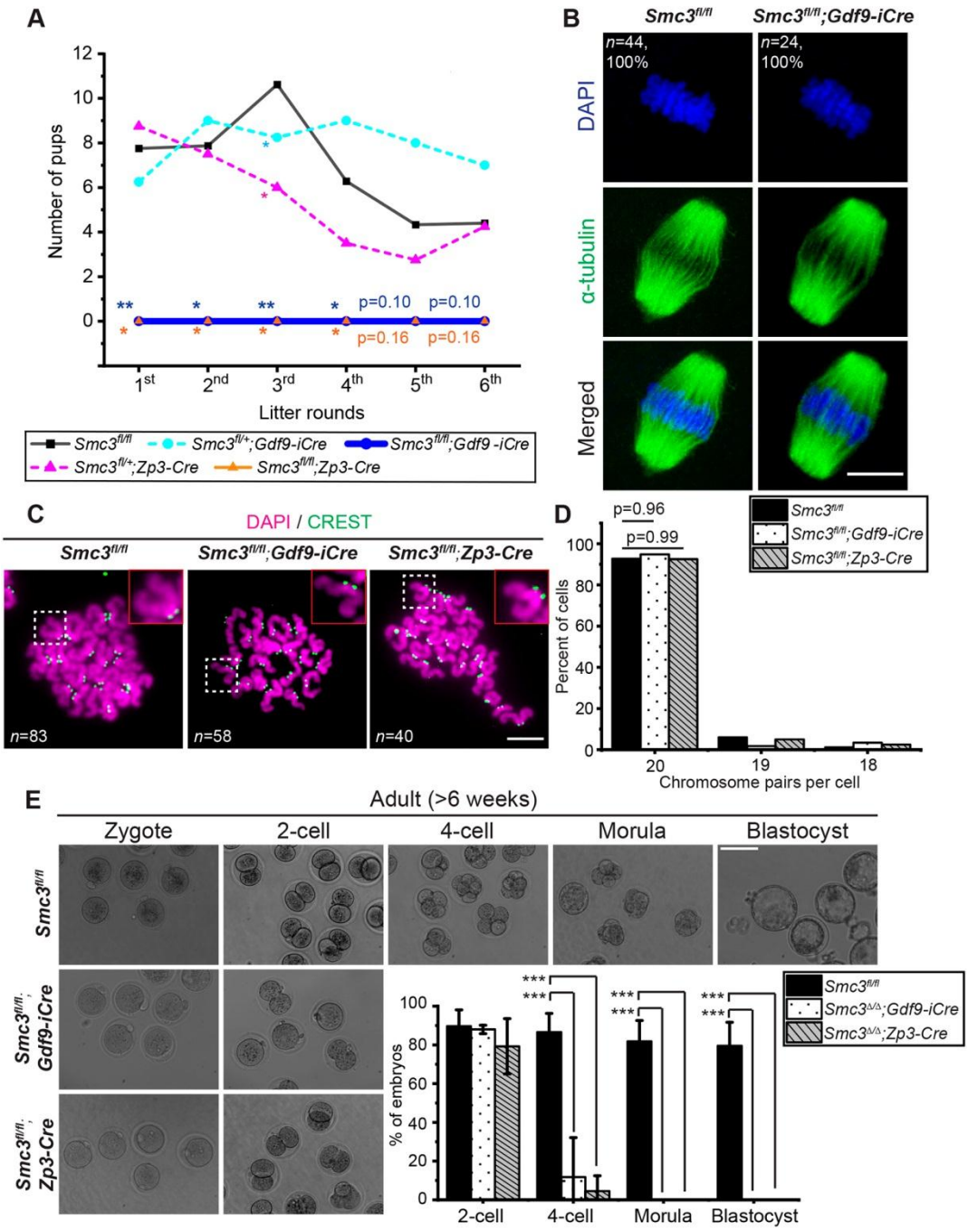

Figure 1. Maternal *Smc3* is essential for embryogenesis but not meiosis. A) Conditional deletion of *Smc3* in mouse oocytes using *Gdf9-iCre* and *Zp3-Cre* and its effect on female fertility. Each female was crossed to produce multiple litters to examine the effect of age on fertility. n=3-8 mice for each genotype, with the mean plotted. The number of pups from each breeder is shown in **Table 1**. *Mann-Whitney U* test was

Development • Accepted manuscript

performed to examine statistical significance between genotypes compared to the wild type (*Smc3*$^{fl/fl}$) at each litter round. *, p < 0.05. **, p < 0.01. **B)** Metaphase II oocytes from adult *Smc3*$^{fl/fl}$ and *Smc3*$^{fl/fl}$*;Gdf9-iCre* female mice were fixed and stained with DAPI and α-tubulin antibody to examine chromosome and spindle fiber structures. Although many oocytes were collected from multiple animals (*n*=44 oocytes from 6 animals for *Smc3*$^{fl/fl}$ and n=24 oocytes from 5 animals for *Smc3*$^{fl/fl}$*;Gdf9-iCre*), we assess only cases with the spindle in a favorable orientation. Scale bar, 20 µm. **C)** Chromosome spreads were performed from metaphase II oocytes from female mice of indicated genotype. Chromosomes were stained with DAPI and kinetochore antibody (CREST) to score chromosome number. Scale bar, 20 µm. n= 6 animals for *Smc3*$^{fl/fl}$, 6 for *Smc3*$^{fl/fl}$*;Gdf9-iCre*, and 3 for *Smc3*$^{fl/fl}$*;Zp3-Cre*. ***D*)** Quantification of number of chromosome pairs from **Fig. 1C**. Chi-square test was performed to examine statistical significance between genotype groups. **E)** Zygotes from *Smc3*$^{fl/fl}$, *Smc3*$^{fl/fl}$*;Gdf9-iCre*, and *Smc3*$^{fl/fl}$*;Zp3-Cre* adult female mice were isolated and cultured *in vitro* to score early embryogenesis. The percent of embryos that progressed to each stage is shown at the lower right panel. *n*=3-8 repeats from each genotype. The total number of scored embryos is shown in **Table 2**. Statistical data are represented with mean ± standard deviation. An unpaired two-tailed student t-test was used to determine statistically significant differences between genotypes. ***, p < 0.001. Scale bar, 100 µm.

Development • Accepted manuscript

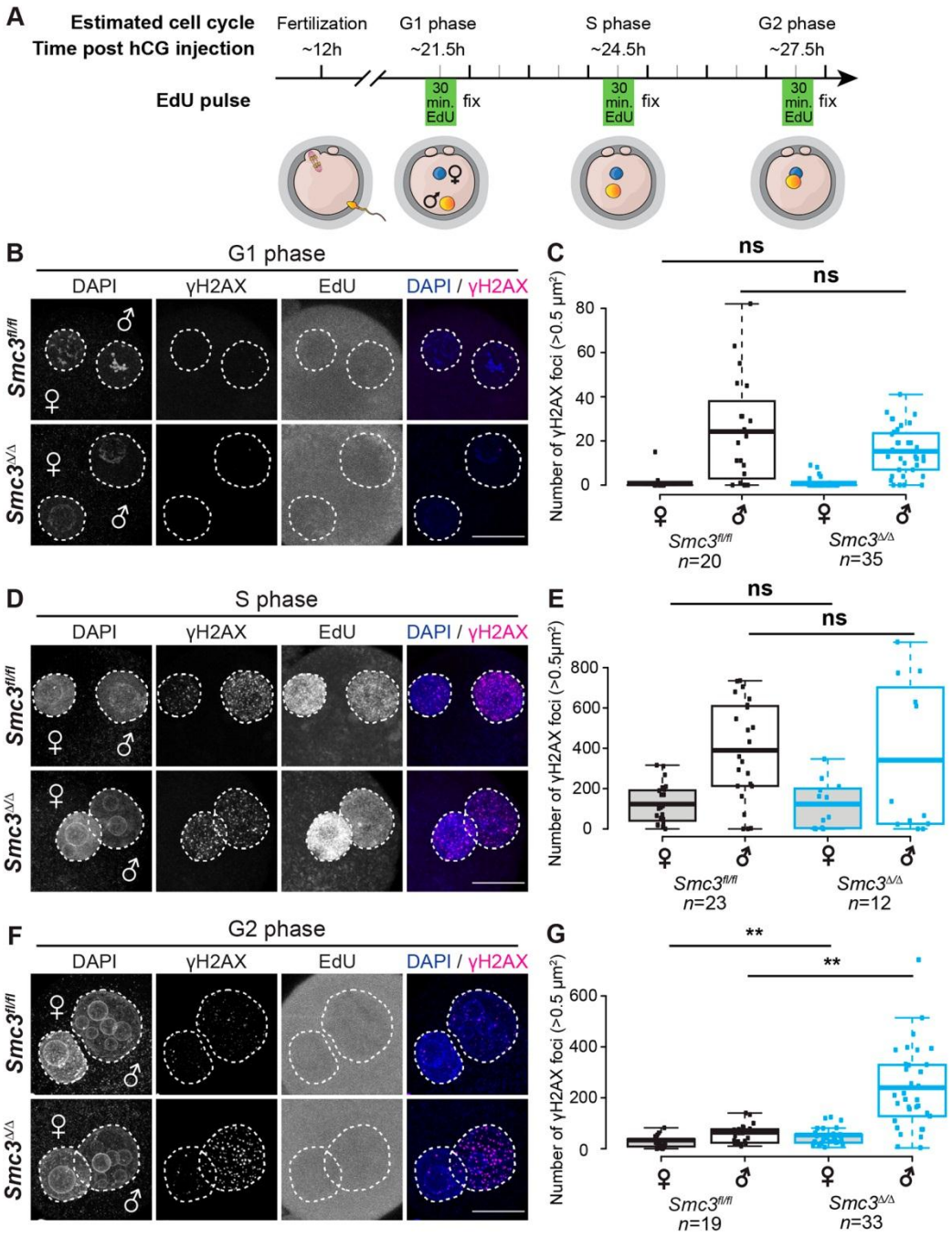

Figure 2. Spontaneous DNA lesions are elevated in *Smc3*$^{\Delta/\Delta}$ *cKO* zygotes following DNA replication. A) Cartoon explaining experimental design and staging. Zygotes from adult *Smc3*$^{fl/fl}$ and *Smc3*$^{\Delta/\Delta}$ *cKO* female mice were isolated, cultured *in vitro* and fixed at the indicated time point. Cell cycle stage was determined by incubation with EdU 30 min prior to fixation. Zygotes were scored using the Click-iT assay and labeled with γH2AX (magenta) and DAPI (blue) in **B**-**G**. **B)** Immunostaining of *Smc3*$^{fl/fl}$ and *Smc3*$^{\Delta/\Delta}$ *cKO* G1 phase zygotes is shown. **C)** Quantification of γH2AX foci in

Development • Accepted manuscript

Smc3$^{fl/fl}$ and *Smc3*$^{\Delta/\Delta}$ *cKO* G1 phase zygotes is shown. **D)** Immunostaining of S phase zygotes from adult *Smc3*$^{fl/fl}$ and *Smc3*$^{\Delta/\Delta}$ *cKO* female mice is shown. **E)** Quantification of γH2AX foci in *Smc3*$^{fl/fl}$ and *Smc3*$^{\Delta/\Delta}$ *cKO* S phase zygotes is shown. **F)** Immunostaining of *Smc3*$^{fl/fl}$ and *Smc3*$^{\Delta/\Delta}$ *cKO* G2 phase zygotes. **G)** Quantification of γH2AX foci in *Smc3*$^{fl/fl}$ and *Smc3*$^{\Delta/\Delta}$ *cKO* G2 phase zygotes. Statistical data are represented with mean (center line) with scatter plot. The box limits indicate the range of 1st/3rd quartile and whiskers extend 1.5 times the interquartile range away from the 1st and 3rd quartile. *Mann-Whitney U* test was performed to examine statistical significance between genotypes. **, $p < 0.01$. Scale bar, 20 μm.

Development • Accepted manuscript

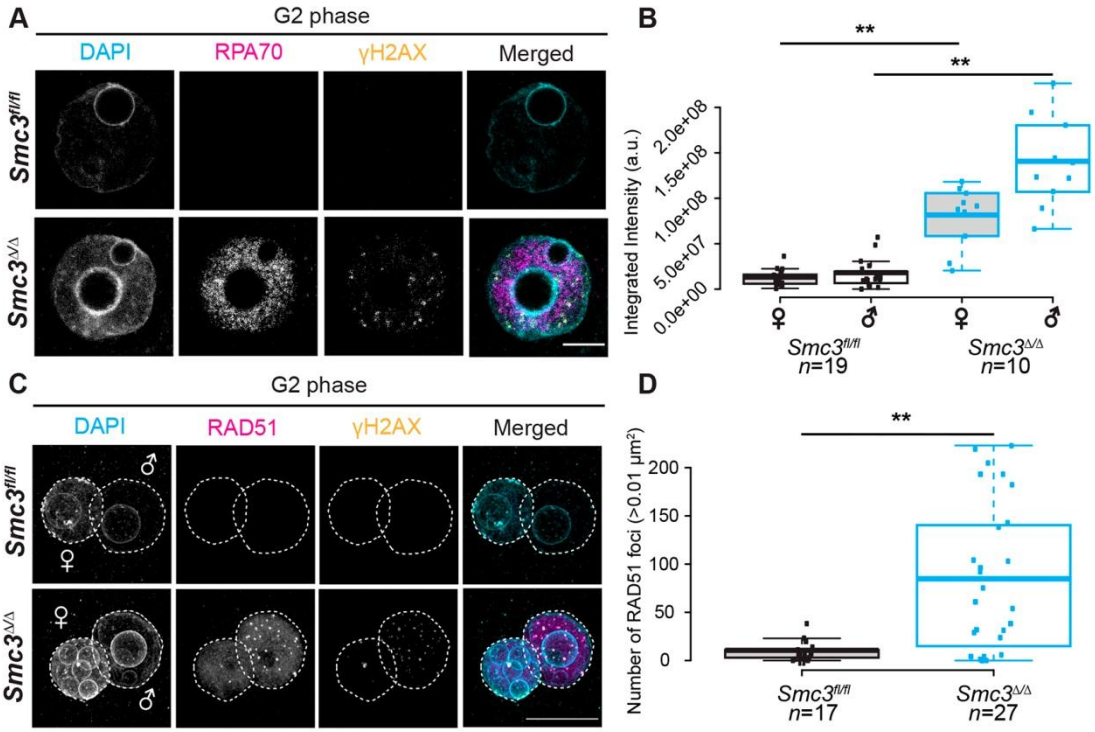

Figure 3. Loss of maternal *Smc3* is associated with persistent DNA lesions in zygotes. G2 phase zygotes were isolated, cultured *in vitro*, incubated with EdU, and fixed as mentioned in **Fig. 2**. **A)** Immunostaining of G2 phase zygotes from adult *Smc3*$^{fl/fl}$ and *Smc3*$^{\Delta/\Delta}$ *cKO* female mice for RPA70 (magenta), γH2AX (yellow), and DAPI (cyan) is shown. Scale bar, 10 μm. **B)** Quantification of the integrated intensity of RAP70 in *Smc3*$^{fl/fl}$ and *Smc3*$^{\Delta/\Delta}$ *cKO* G2 phase zygotes is shown. **C)** Immunostaining of G2 phase zygotes from adult *Smc3*$^{fl/fl}$ and *Smc3*$^{\Delta/\Delta}$ *cKO* female mice for RAD51 (magenta), γH2AX (yellow), and DAPI (cyan) is shown. Scale bar, 20 μm. **D)** Quantification of RAD51 foci in *Smc3*$^{fl/fl}$ and *Smc3*$^{\Delta/\Delta}$ *cKO* G2 phase zygotes is shown. Statistical data are represented with mean (center line) with scatter plot, with box limits as in Figure 2G. *Mann-Whitney U* test was performed to examine statistical significance between genotypes. **, $p < 0.01$.

Development • Accepted manuscript

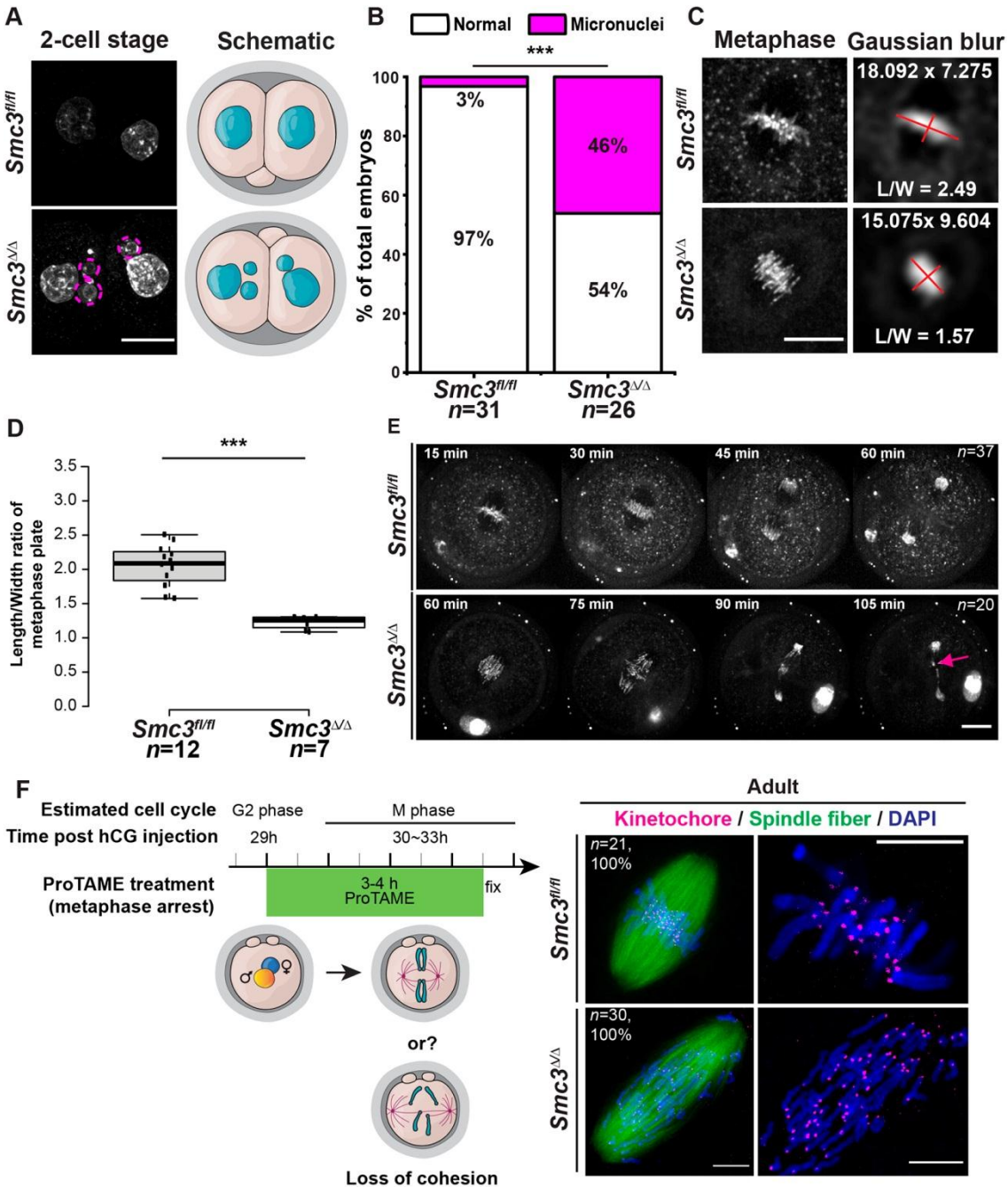

Figure 4. Loss of maternal *Smc3* is associated with micronuclei and lagging chromosomes during the first mitotic division. A) DAPI staining for 2-cell stage embryos from adult *Smc3*$^{fl/fl}$ and *Smc3*$^{\Delta/\Delta}$ *cKO* female mice is shown. Dotted circles indicate micronuclei. A schematic cartoon is presented on the right panel for each genotype. Scale bar, 10 µm. **B)** Quantification of micronuclei positive 2-cell stage embryos from adult *Smc3*$^{fl/fl}$ and *Smc3*$^{\Delta/\Delta}$ *cKO* female mice is shown. A Chi-square test was performed to determine statistical significance between genotypes. ***, $p < 0.001$.

Development • Accepted manuscript

C-E) Live-cell imaging of the SIR-DNA dye-stained zygotes revealed that **(C-D)** chromosome morphologies were different and **(E)** micronuclei were derived from lagging chromosome during the first mitotic division in *Smc3*$^{\Delta/\Delta}$ *cKO* zygotes. **C)** The Z projection of spindle chromosomes is Gaussian blurred and the length and width are measured. Red lines indicate the length and width of spindle chromosomes. Scale bar, 10 µm. **D)** Quantification of length/width (L/W) ratio of spindle chromosomes in *Smc3*$^{fl/fl}$ and *Smc3*$^{\Delta/\Delta}$ metaphase zygotes is shown. Only embryos with proper orientation were counted. Statistical data are represented with mean (center line) with scatter plot, with box limits as in Figure 2G. An unpaired two-tailed student t-test was performed to examine statistical significance between genotypes. ***, $p < 0.001$. **E)** The time-lapse montages of *Smc3*$^{fl/fl}$ and *Smc3*$^{\Delta/\Delta}$ zygotes are shown. The magenta arrow indicates the micronucleus formed from lagging chromosomes. Scale bar, 20 µm. See **Movie 1** and **Movie 2** for the entire process at high resolution. **F)** Immunostaining of metaphase zygotes from adult *Smc3*$^{fl/fl}$ and *Smc3*$^{\Delta/\Delta}$ *cKO* animals for kinetochores (CREST), spindle fibers (α-tubulin), and chromosomes (DAPI) is shown. *In vitro* cultured zygotes were incubated with ProTAMEto synchronize/arrest at metaphase. (n, *Smc3*$^{fl/fl}$=21, *Smc3*$^{\Delta/\Delta}$=30). Magnified images of kinetochore and chromosomes are presented on the right panel. Scale bar, 10 µm.

Development • Accepted manuscript

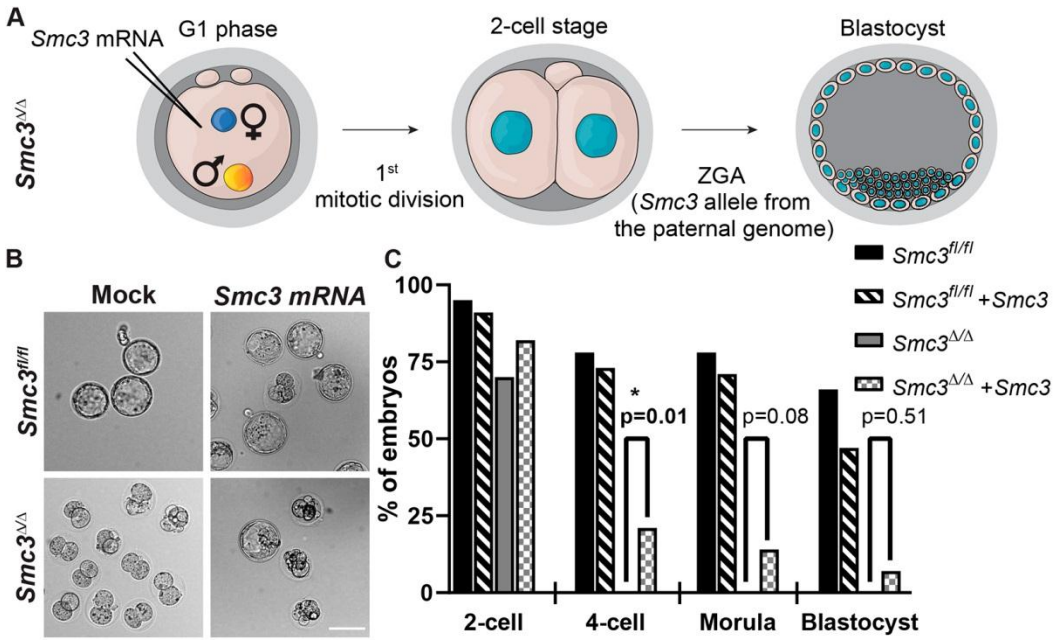

Figure 5. Developmental competence of the *Smc3$^{\Delta/\Delta}$ cKO* zygote is rescued by microinjection of *Smc3*. **A)** Cartoon explaining the experimental design and staging. *Smc3* mRNA or TE buffer (mock) was microinjected into the ***Smc3$^{\Delta/\Delta}$*** *cKO* zygote in G1 phase**.** If the mutant zygotes successfully complete the first mitotic division, *Smc3* expressed from the paternal genome should enable embryogenesis after ZGA. **B)** Microinjected embryos were cultured *in vitro*. **C)** The quantification of early embryogenesis is shown, as a percent of zygotes that successfully progressed to the stage indicated. The total number of embryos at each stage is shown in **Table 3**. Fisher's exact test was performed to examine statistical significance between indicated genotypes at each stage. *, $p < 0.05$.

Development • Accepted manuscript

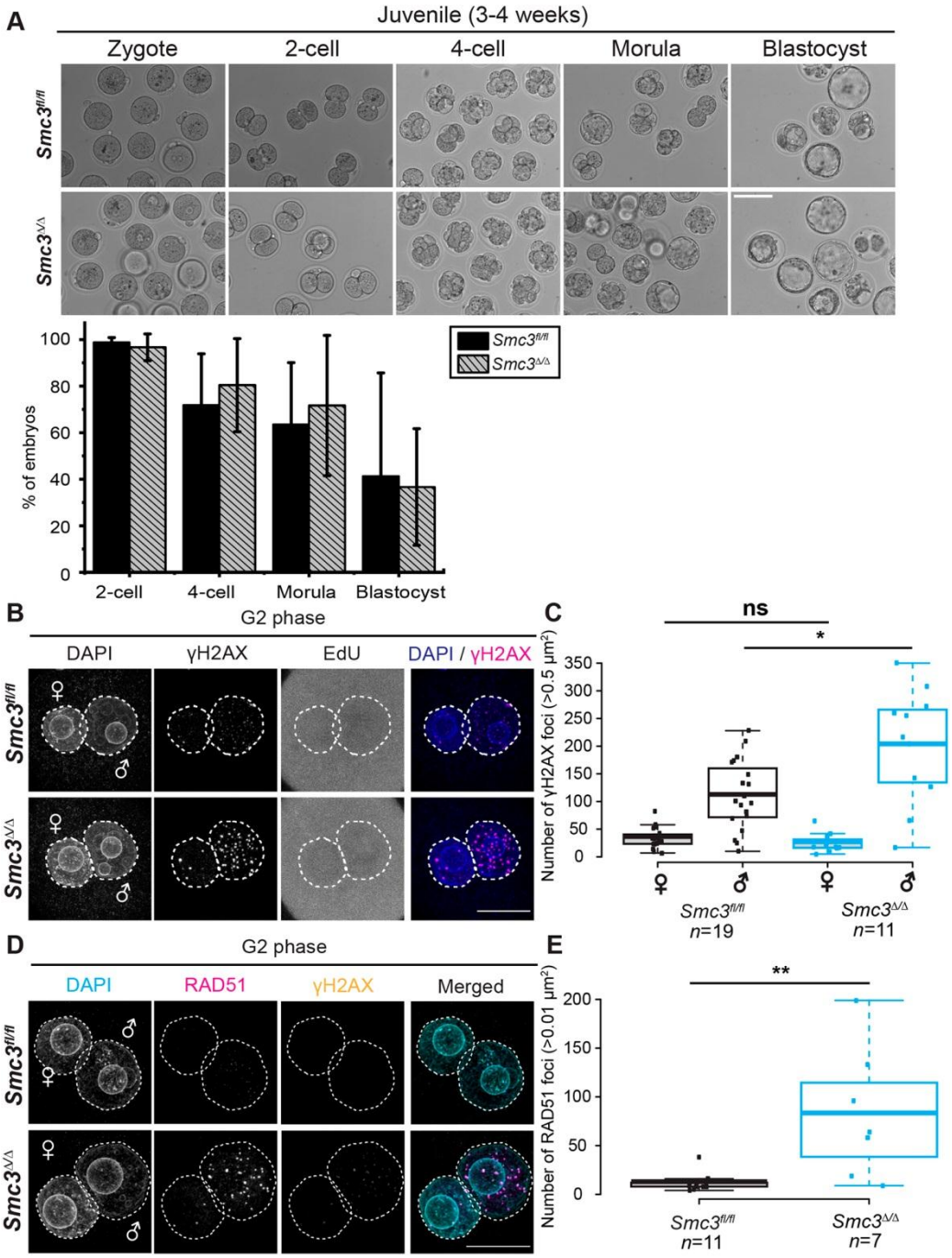

Figure 6. Developmental competence of the *Smc3$^{\Delta/\Delta}$ cKO* zygote is enabled in juvenile females (3-4 weeks). **A)** Embryos from juvenile females of the indicated genotype were cultured *in vitro* for the indicated length of time following the condition in **Fig. 1E**. The quantification of early embryogenesis is shown in the lower histogram. *n*=3 repeats from each genotype. The total number of embryos scored at each stage is shown in **Table 4**. Statistical data are represented by the mean ± standard deviation. An unpaired two-tailed student t-test was used and show no statistically significant

Development • Accepted manuscript

differences between genotypes. Scale bar, 100 µm. **B)** Zygotes in G2 phase, derived from juvenile females with the indicated genotype, were immunostained for γH2AX as described in **Fig. 2**. Scale bar, 20 µm. **C)** Quantification of γH2AX foci from the conditions in (B) is shown. *Mann-Whitney U* was performed to determine statistical significance between genotypes. *, $p < 0.05$. **D)** G2 phase zygotes from juvenile females of the indicated genotype were immunostained for RAD51(magenta), γH2AX (yellow), and DAPI (cyan). Scale bar, 20 µm. **E)** Quantification of RAD51 foci in juvenile *Smc3*$^{fl/fl}$ and *Smc3*$^{\Delta/\Delta}$ *cKO* G2 phase zygotes from (D) is shown. Data in **6C)** and **6E)** are represented with mean (center line) and scatter plot with box limits as in Figure 2G.*Mann-Whitney U* test was performed to determine statistical significance between genotypes. **, $p < 0.01$.

Development • Accepted manuscript

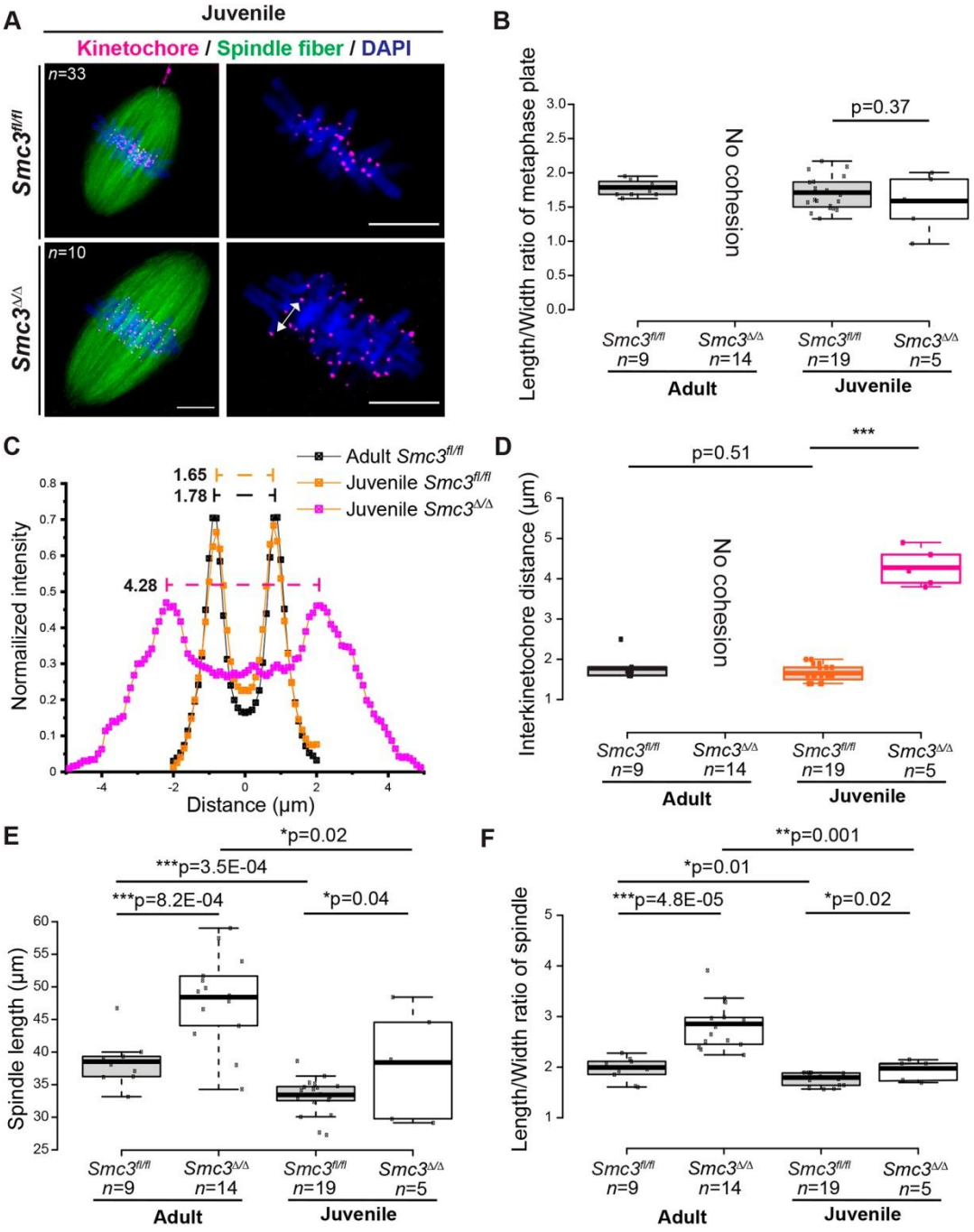

Figure 7. Loss of maternal *Smc3* disrupts sister-chromatid cohesion during the first mitotic division. Zygotes cultured *in vitro* from adult and juvenile *Smc3*$^{fl/fl}$ and *Smc3*$^{\Delta/\Delta}$ *cKO* female mice were incubated with an APC inhibitor to arrest at metaphase. **A)** Metaphase arrested and fixed zygotes from juvenile *Smc3*$^{fl/fl}$ and *Smc3*$^{\Delta/\Delta}$ *cKO* female mice were stained to visualize kinetochores (CREST, magenta), spindle fibers (α-tubulin, green), and DNA (DAPI, blue). Compared to **Fig. 4D,** the phenotype between adult and juvenile *Smc3*$^{\Delta/\Delta}$ zygotes is easily distinguished. The bi-headed arrow

Development • Accepted manuscript

indicates separated centromeres from an individual sister chromatid pair. Scale bar, 10 μm. **B)** Quantification of L/W ratio of spindle chromosomes from adult **(Fig. 4F)** and juvenile **(Fig. 7A)** *Smc3*$^{fl/fl}$ and *Smc3*$^{\Delta/\Delta}$ metaphase zygotes is shown. Metaphase zygotes were incubated with the APC inhibitor. Only the embryos with proper orientation were counted into quantification. **C)** The interkinetochore distance was measured by centromere signals between individual sister chromatid pairs. Line profiles of the CREST signal along the x axis were generated from aligning chromosome centers of each chromosome pair shown in **Fig. 7A** and **Fig. 4F**. The average profile of all chromosome pairs in individual zygotes was then generated by fitting line profiles to a double gaussian model**.** The two peaks of CREST signal determined the position of centromere centers. The dotted line indicates the interkinetochore distance of chromosome pairs in indicated genotypes. The sample size is indicated in **Fig. 7D**. **D)** Quantification of the interkinetochore distance in metaphase zygotes from adult and juvenile *Smc3*$^{fl/fl}$ and *Smc3*$^{\Delta/\Delta}$ *cKO* female mice. The interkinetochore distance is determined as in **Fig 7C**. The interkinetochore distance of adult *Smc3*$^{\Delta/\Delta}$ *cKO* zygotes cannot be quantified since cohesion is completely lost and sister chromatid pairs are indistinguishable. **E-F)** Quantifications of length **(E)** and L/W ratio **(F)** of spindle from adult and juvenile are shown. Data are represented with mean (center line) and scatter plot, with box limits as in **Fig. 2G**. A one-way ANOVA test with the Tukey HSD test was used to determine statistically significant differences between genotypes in **Fig 7D**. Unpaired two-tailed student t-tests were performed to examine statistical significance between groups in **Fig. 7B, E, and F**. *, $p<0.05$. **, $p<0.01$. ***, $p<0.001$.

Development • Accepted manuscript

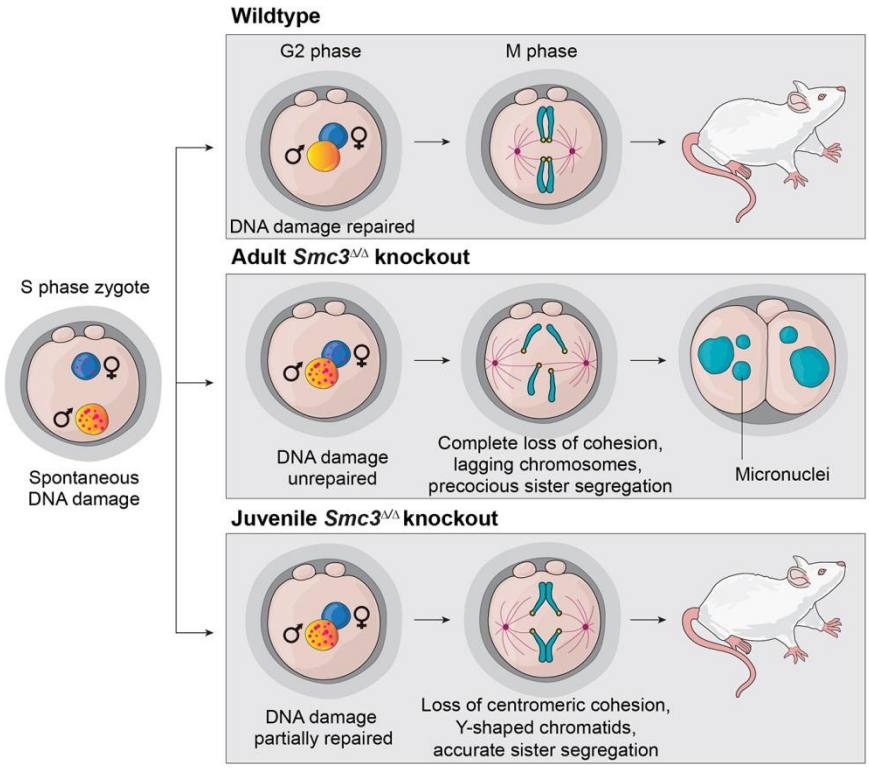

Figure 8. A schematic summary of results highlights significant findings. Spontaneous DNA lesions accumulated following S phase in adult-derived *Smc3*$^{\Delta/\Delta}$ *cKO* zygotes, followed by the first mitotic division with lagging chromosomes, micronuclei, and arrest at the 2-cell stage. Cohesion is undetectable in adult-derived *Smc3*$^{\Delta/\Delta}$ *cKO* zygotes. While juvenile-derived *Smc3*$^{\Delta/\Delta}$ *cKO* zygotes lose centromeric cohesion, they can sustain developmental competence with cohesion in the q-arms.

Development • Accepted manuscript

Table 1. Female fertility from conditional deletion of *Smc3* in mouse oocytes from juvenile and adult female mice. Each female breeder was continuously crossed to produce multiple litters to score litter size and fertility. *Mann-Whitney U* test was performed to examine statistical significance of pups per litter between genotypes.

	Number of pups									
Genotype	**1st Litter**	**2nd Litter**	**3rd Litter**	**4th Litter**	**5th Litter**	**6th Litter**	**Total**	**Pups per litter**	**Mean of Pups per litter**	**p-value**
Smc3$^{fl/fl}$	8	9	9	10	12	10	58	9.67	7.58	
	8	0	10	3	7	9	37	6.17		
	12	10	9	0	0	0	31	5.17		
	10	9	13	8	0	0	40	6.67		
	8	11	12	sacrificed			31	10.33		
	1	8	10	10	10	9	48	8.00		
	7	8	11	12	0	0	38	6.33		
	8	8	11	1	9	13	50	8.33		
Smc3$^{fl/+}$;Gdf9-iCre	8	10	7	8	7	5	45	7.50	7.92	0.799
	6	10	7	8	7	7	45	7.50		
	5	8	9	10	13	9	54	9.00		
	6	8	10	10	5	7	46	7.67		
Smc3$^{fl/fl}$;Gdf9-iCre	0	0	0	0	0	0	0	0.00	0.00	**0.007**
	0	0	0	0	0	0	0	0.00		
	0	0	0	0	0	0	0	0.00		
	0	0	0	0	0	0	0	0.00		
Smc3$^{fl/+}$;Zp3-Cre	8	6	8	4	6	11	43	7.17	5.63	0.214
	7	9	10	10	5	6	47	7.83		
	11	8	0	0	0	0	19	3.17		
	9	11	6	0	0	0	26	4.33		
Smc3$^{fl/fl}$;Zp3-Cre	0	0	0	0	0	0	0	0.00	0.00	**0.018**
	0	0	0	0	0	0	0	0.00		
	0	0	0	0	0	0	0	0.00		

Development • Accepted manuscript

Table 2. Quantification of embryogenesis of zygotes cultured *in vitro* from adult *Smc3*$^{fl/fl}$ and *Smc3*$^{fl/fl}$*;Gdf9-iCre*, and *Smc3*$^{fl/fl}$*;Zp3-Cre* female mice. Only fertilized zygotes with a visible pronucleus were isolated for culture *in vitro* and all unfertilized oocytes were discarded. Samples were scored every day. N>3 mice per indicated genotype. Fisher's exact test was performed to examine statistical significance between the wild type and mutants at each stage.

		Number of embryos (%) (p-value)				
Genotype	**Age**	**Zygote**	**2-cell**	**4-cell**	**Morula**	**Blastocyst**
***Smc3*$^{fl/fl}$**	>6 weeks (Adult)	157	139 (88.5)	133 (84.7)	126 (80.3)	123 (78.3)
Smc3*$^{fl/fl}$*;Gdf9-iCre		27	24 (88.9) (1)	6 (22.2) (2.04e-10)	0 (0) (7.07e-12)	0 (0) (9.05e-16)
Smc3*$^{fl/fl}$*;Zp3-Cre		64	51 (79.7) (0.09)	3 (4.7) (<2.2e-16)	0(0) (< 2.2e-16)	0 (0) (< 2.2e-16)

Table 3. Embryogenesis of microinjected zygotes cultured *in vitro* from adult *Smc3*$^{fl/fl}$ and *Smc3*$^{fl/fl}$*;Zp3-Cre* female mice. Microinjection of *Smc3* mRNA or TE buffer (mock) was performed in G1 phase. Embryos from adult female mice with indicated genotypes were isolated for culture *in vitro* as described for **Table 2**. All embryos were collected and scored from 4 experimental replicates in total. Embryos were isolated from 13 *Smc3*$^{fl/fl}$ and 8 *Smc3*$^{\Delta/\Delta}$ *cKO* female mice. Fisher's exact test was performed to examine statistical significance between indicated genotypes at each stage.

		Number of embryos (%)				
Genotype	**Microinjection**	**Zygote**	**2-cell**	**4-cell**	**Morula**	**Blastocyst**
***Smc3*$^{fl/fl}$**	Mock	42	40 (95.2)	33 (78.6)	33 (78.6)	28 (66.7)
***Smc3*$^{fl/fl}$**	*Smc3* mRNA	87	80 (92.0) (1)	64 (73.6) (0.89)	62 (71.3) (0.78)	41 (47.1) (0.28)
Smc3*$^{fl/fl}$*;Zp3-Cre	Mock	31	22 (71.0)	0 (0)	0 (0)	0 (0)
Smc3*$^{fl/fl}$*;Zp3-Cre	*Smc3* mRNA	41	34 (82.9) (0.72)	9 (22.0) (0.01)	6 (14.6) (0.08)	2 (4.9) (0.51)

Development • Accepted manuscript

Table 4. Quantification of embryogenesis of zygotes cultured *in vitro* from juvenile *Smc3*$^{fl/fl}$ and *Smc3*$^{fl/fl}$*;Zp3-Cre* female mice. Embryos from female mice with indicated genotypes were isolated for culture *in vitro* as described for **Table 2**. N>3 mice per indicated genotype. Fisher's exact test was performed to examine statistical significance between indicated genotypes at each stage.

		Number of embryos (%) (p-value)				
Genotype	**Age**	**Zygote**	**2-cell**	**4-cell**	**Morula**	**Blastocyst**
***Smc3*$^{fl/fl}$**	3-4 weeks (Juvenile)	63	62 (98.4)	45 (71.4)	38 (60.3)	25 (40.0)
Smc3*$^{fl/fl}$*;Zp3-Cre		60	58 (96.7) (0.61)	46 (76.7) (0.54)	40 (66.7) (0.57)	28 (46.7) (0.47)

Development • Accepted manuscript

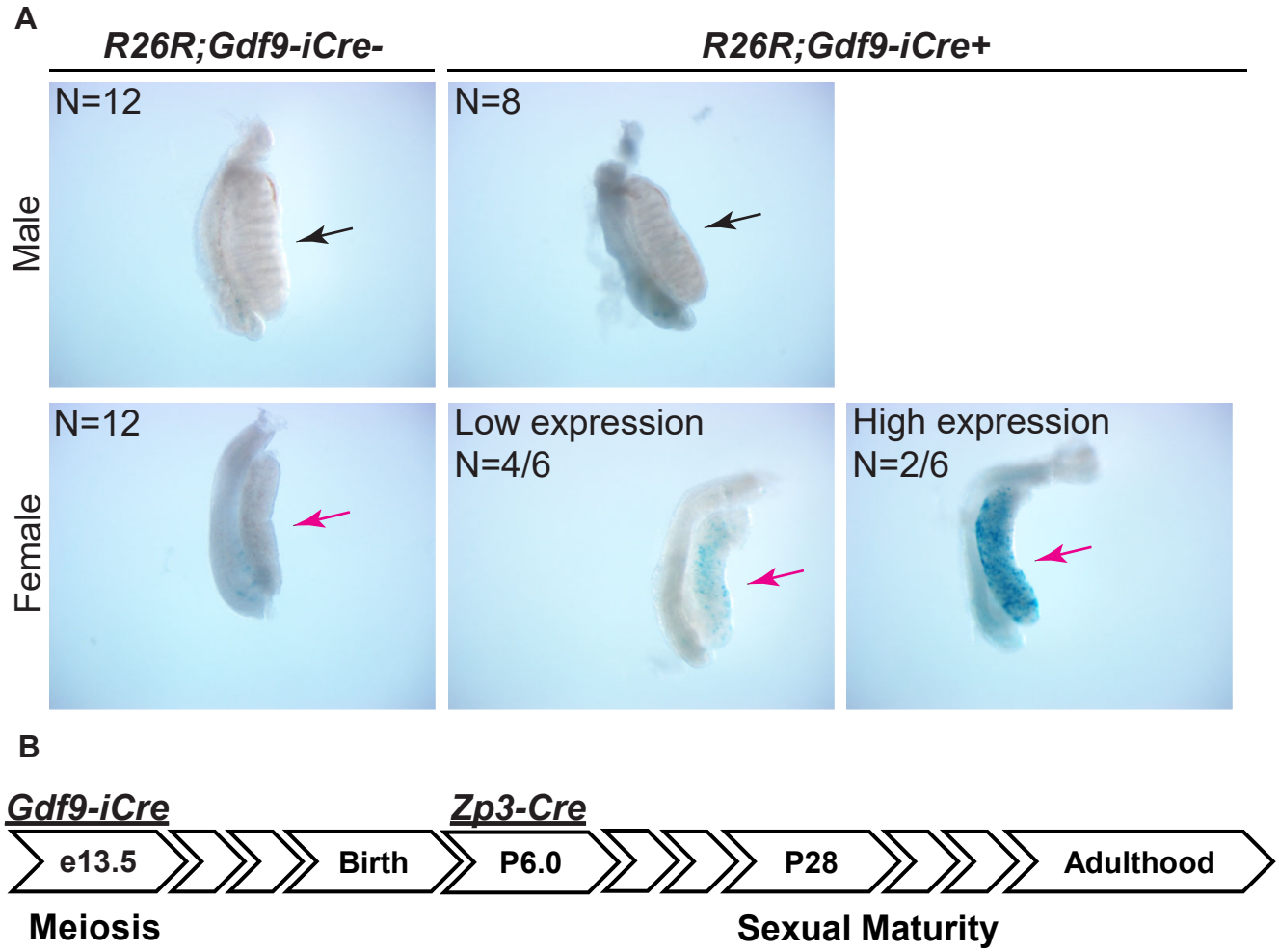

Fig. S1. *Gdf9-iCre* is expressed in the female gonad at 13.5 *dpc*. A) *Gt(ROSA)26Sor*$^{tm1(LacZ)Cos}$ (known as *R26R*) females were crossed with *Gdf9-iCre*$^{+}$ males The STOP sequence is removed and the downstream lacZ gene is expressed in cells/ tissues where cre is expressed. β-gal staining in mouse gonads at 13.5 *dpc* was detected using X-gal. Male gonads and *cre* negative gonads were tested as negative controls; female gonads with *Cre*$^{+}$ showed β-gal staining. *n*=12 for *R26R* male gonads, 8 for *R26R Gdf9-iCre*$^{+}$ male gonads, 12 for *R26R* female gonads, and 6 for *R26R Gdf9-iCre*$^{+}$ female gonads. Black arrows indicate representative male gonads. Magenta arrows indicate representative female gonads. Sex is determined by morphology of the gonad and genotyping of the embryo. **B)** A schematic of Cre driver expression in relation to mouse development.

Development • Supplementary information

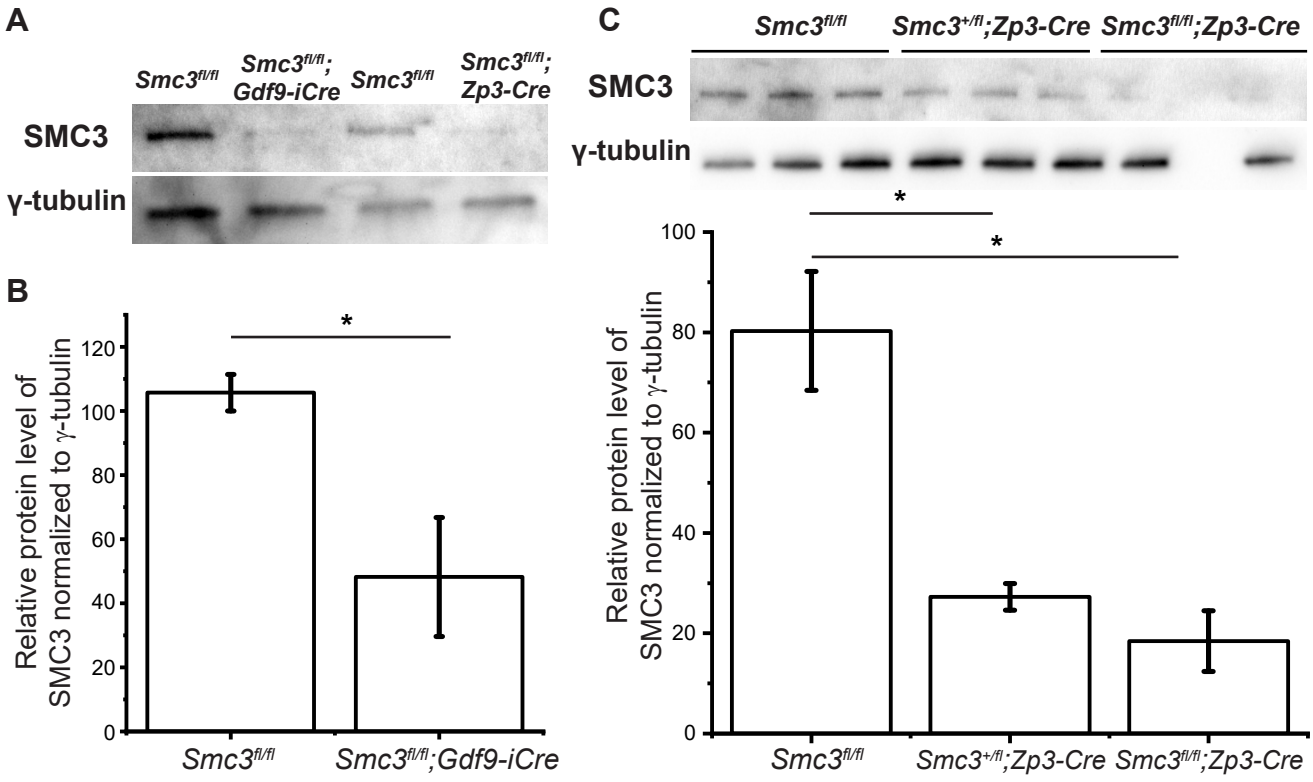

Fig. S2. Maternal SMC3 deprived from oocytes by *Gdf9-iCre and Zp3-Cre* drivers. Related to Fig. 1. Fully grown germinal vesicles (GV) stage oocytes were collected and snap frozen from ovaries of PMSG-stimulated adult female mice (6-8-week-old). The level of SMC3 was examined and γ-Tubulin was used as the loading control. *n*=30 oocytes per lane. **A)** A representative western blot is shown for oocytes from *Smc3*$^{fl/fl}$, *Smc3*$^{fl/fl}$*;Gdf9-iCre*, and *Smc3*$^{fl/fl}$*;Zp3-Cre* female mice. **B)** Quantification of the level of SMC3 in *Smc3*$^{fl/fl}$ and *Smc3*$^{fl/fl}$*;Gdf9-iCre* oocytes is shown (*n*, *Smc3*$^{fl/fl}$=4, *Smc3*$^{fl/fl}$*;Gdf9-iCre*=5). **C)** Western blots and their corresponding quantification from oocytes derived from *Smc3*$^{fl/fl}$ (wild type), *Smc3*$^{+/fl}$*;Zp3-Cre* (heterozygous), and *Smc3*$^{fl/fl}$*;Zp3-Cre* (homozygous) female mice is shown (*n*, *Smc3*$^{fl/fl}$=4, *Smc3*$^{+/fl}$*;Zp3-Cre*=3, *Smc3*$^{fl/fl}$*;Zp3-Cre*=3). The chemiluminescence values quantified by ImageJ are an imperfect reflection of what is observed by eye. Statistical data are represented with mean ± standard deviation. An unpaired two-tailed student t-test was used to determine statistically significant differences between genotypes. *, $p < 0.05$.

Development • Supplementary information

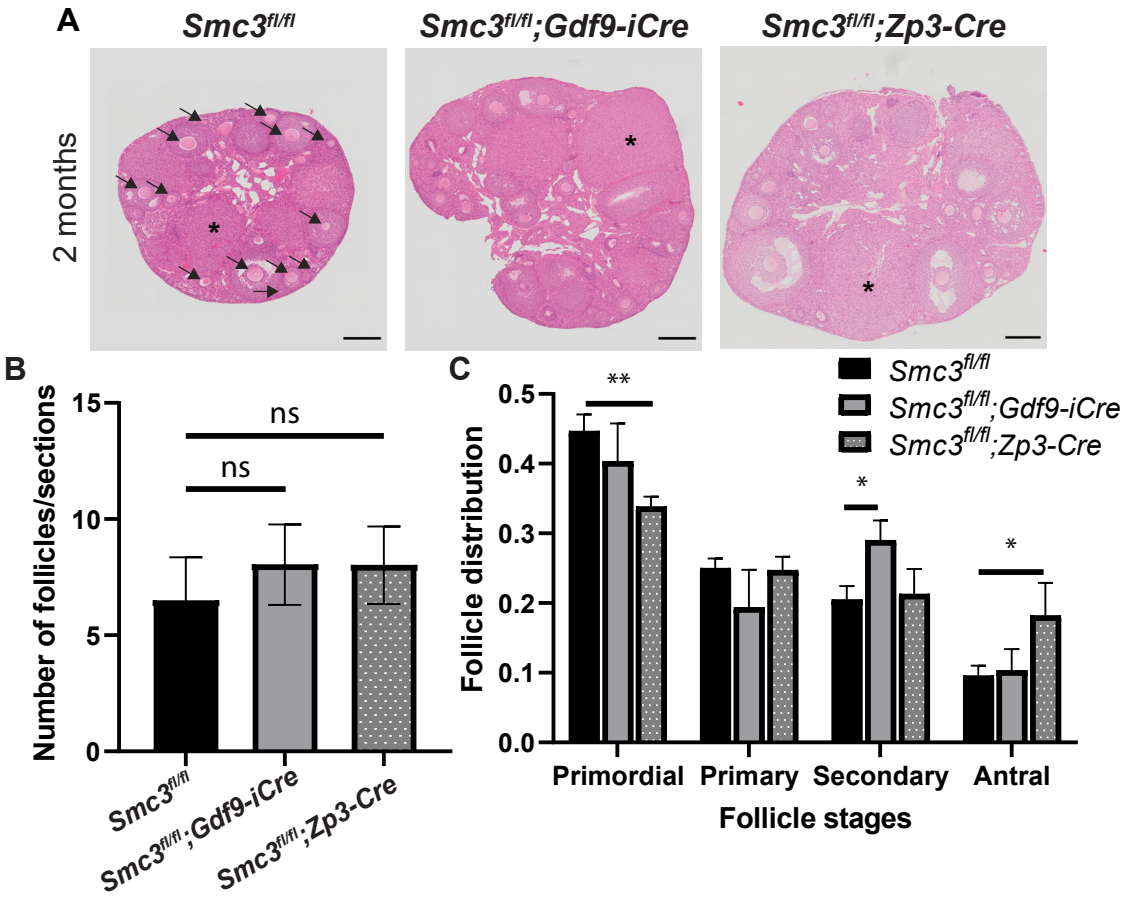

Fig. S3. Removal of maternal *Smc3* from oocytes by either the *Gdf9-iCre* or *Zp3-Cre* drivers does not reduce ovarian reserve. Follicles were scored and categorized in histological sections from the entire ovary. *n*=3 mice for each genotype. **A**) Hematoxylin and eosin staining of histologic sections was performed on ovaries from 2-month-old mice of each genotype. Arrows indicate follicles consisting of an individual oocyte surrounded by granulosa cells. Asterisks indicate the corpus lutea. **B)** Quantification of the total number of follicles in ovaries from 2-month-old *Smc3*$^{fl/fl}$, *Smc3*$^{fl/fl}$*;Gdf9-iCre*, and *Smc3*$^{fl/fl}$*;Zp3-Cre* female mice shows no difference in number as a function of genotype. **C)** The distribution of follicle stages in ovaries from 2-month-old mice is shown as a function of genotype. An unpaired two-tailed student t-test was used to determine statistically significant differences between genotypes. *, $p<0.05$. **, $p<0.01$. Scale bar, 100 μm.

Development • Supplementary information

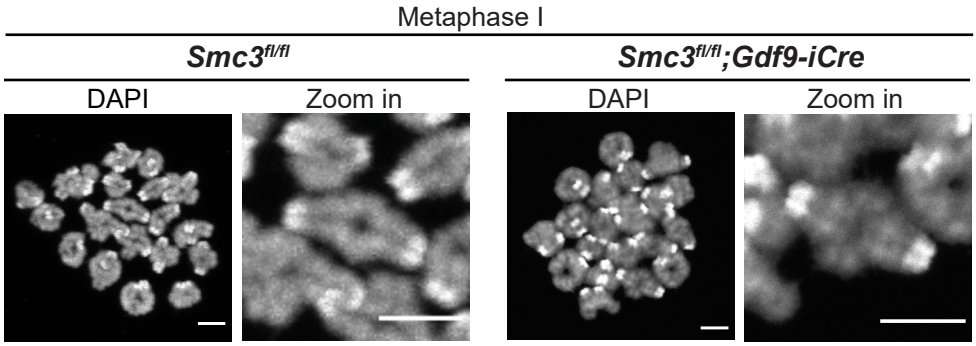

Fig. S4. Meiotic sister chromatid cohesion was not affected in *Smc3*$^{\Delta/\Delta}$*Gdf9-iCre* oocytes in metaphase I. Related to Fig. 1. Chromosome spreads were prepared as described in **Fig. 1**. Intact bivalents showed that sister chromatid cohesion was comparable between *Smc3*$^{fl/fl}$ and *Smc3*$^{fl/fl}$*;Gdf9-iCre* oocytes (*n, Smc3*$^{fl/fl}$=2, *Smc3*$^{fl/fl}$*;Gdf9-iCre*=6). Images were captured by confocal microscope. Scale bar, 5 μm.

Development • Supplementary information

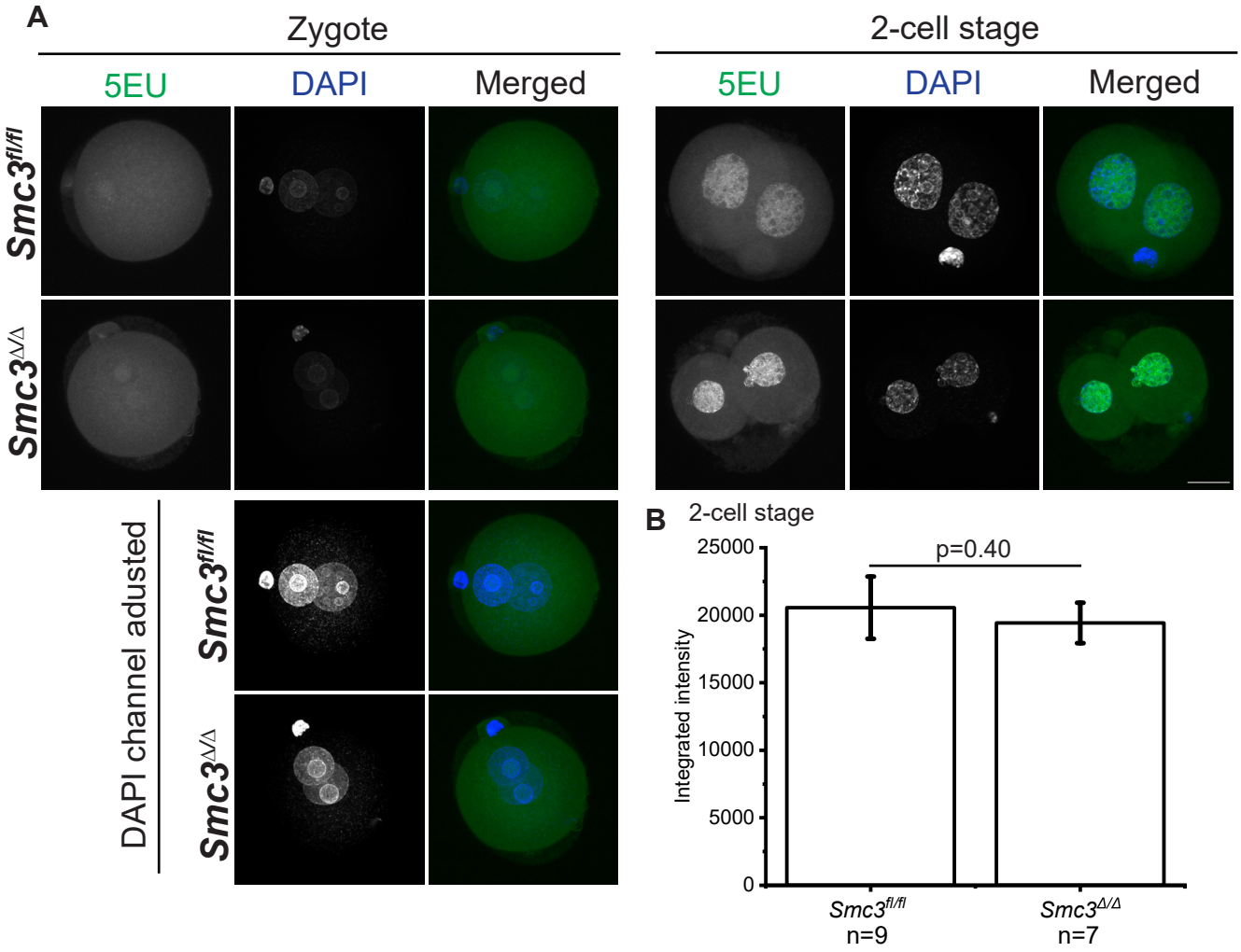

Fig. S5. Zygotic genome activation occurred with normal timing when *Smc3* is depleted. Zygotes from adult *Smc3*$^{fl/fl}$ and *Smc3*$^{\Delta/\Delta}$ *cKO* female mice were incubated with 5EU 2 hours before fixation. **A)** Samples were developed by Click-iT assay (green) and nuclei were labeled with DAPI (blue) *(n, Smc3*$^{fx/fx}$ zygote=10, *Smc3*$^{\Delta/\Delta}$ zygote=12, *Smc3*$^{fx/fx}$ 2-cell stage=9, and *Smc3*$^{\Delta/\Delta}$ 2-cell stage=7). **B)** Integrated intensity of 5EU signal from nuclei was quantified as an indicator of global RNA transcription. Statistical data are represented with mean ± standard deviation. A student t-test was used to determine statistically significant differences between genotypes. Scale bar, 20 μm.

Development • Supplementary information

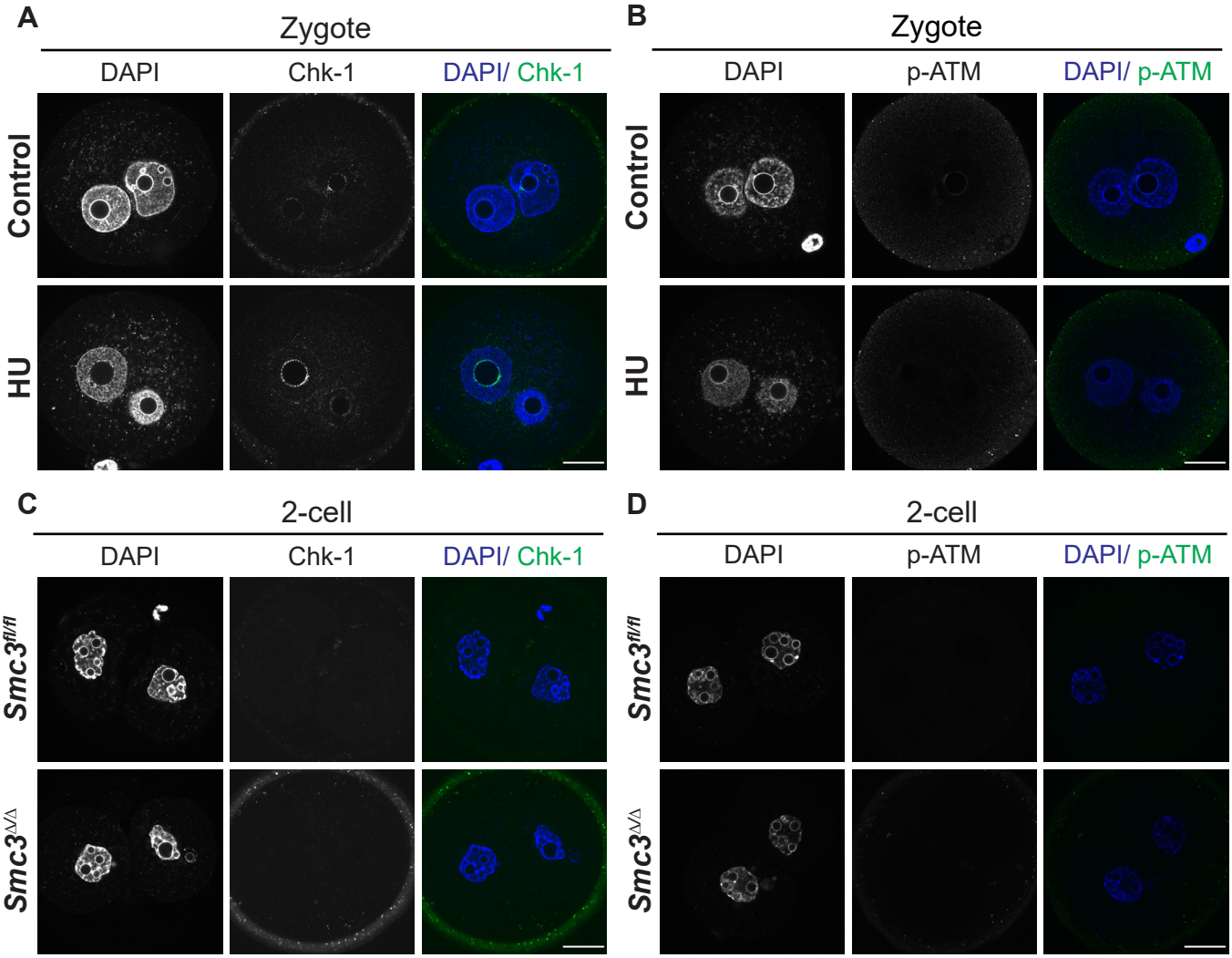

Fig. S6. Canonical ATR and ATM checkpoints are not activated in mutant embryos. A-B) Zygotes from wildtype females were cultured with hydroxyurea (HU) to introduce replication stress. Total Chk1 **(A)** and p-ATM **(B)** were labeled in 28 hpi zygotes (*n*, $Smc3^{fx/fx}$=6, $Smc3^{\Delta/\Delta}$=6 for each immunostaining). **C-D)** Immunostaining of Chk1 **(C)** and p-ATM **(D)** in $Smc3^{fx/fx}$ and $Smc3^{\Delta/\Delta}$ embryos at 2-cell stage (*n*, $Smc3^{fx/fx}$=11, $Smc3^{\Delta/\Delta}$=24 for each immunostaining). Scale bar: 20 μm.

Development • Supplementary information

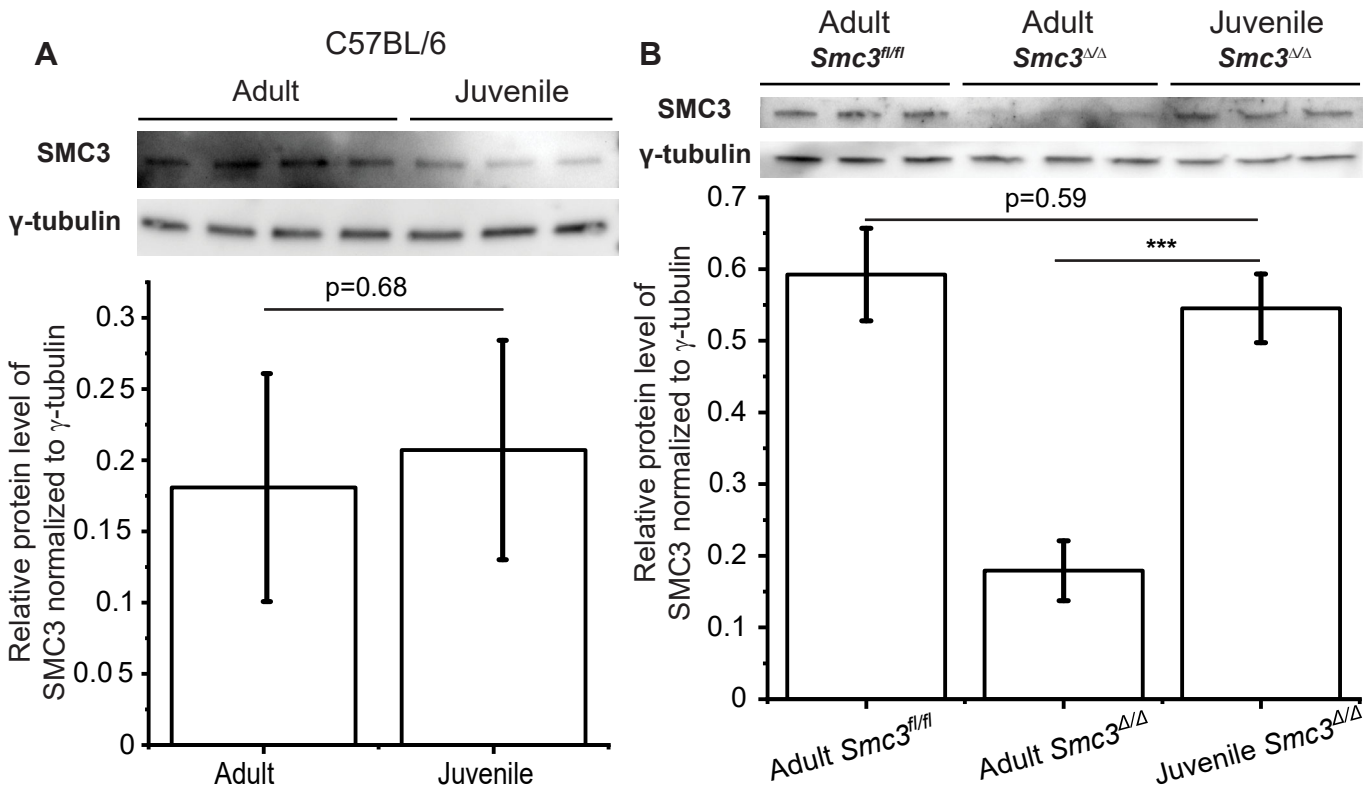

Fig. S7. SMC3 protein levels are sustained in mutant oocytes from juvenile females. Related to Fig. 6. Fully grown GV stage oocytes from adult or juvenile females of the indicated genotypes were collected as described in **Fig. S2**. The level of SMC3 was examined and γ-Tubulin was used as the loading control. *n*=30 oocytes per lane. **A)** Analysis of the western blot of oocytes from adult and juvenile C57BL/6 female mice (*n*=4 replicates for adult and 3 for juvenile). **B)** Analysis of the western blot of oocytes from adult *Smc3*$^{fl/fl}$, adult *Smc3*$^{fl/fl}$*;Zp3-Cre*, and juvenile *Smc3*$^{fl/fl}$*;Zp3-Cre* female mice is shown (*n*=3 per genotype). Statistical data are represented with mean ± standard deviation. An unpaired two-tailed student t-test was used to determine statistically significant differences between genotypes. *, $p < 0.05$. ***, $p < 0.001$.

Development • Supplementary information

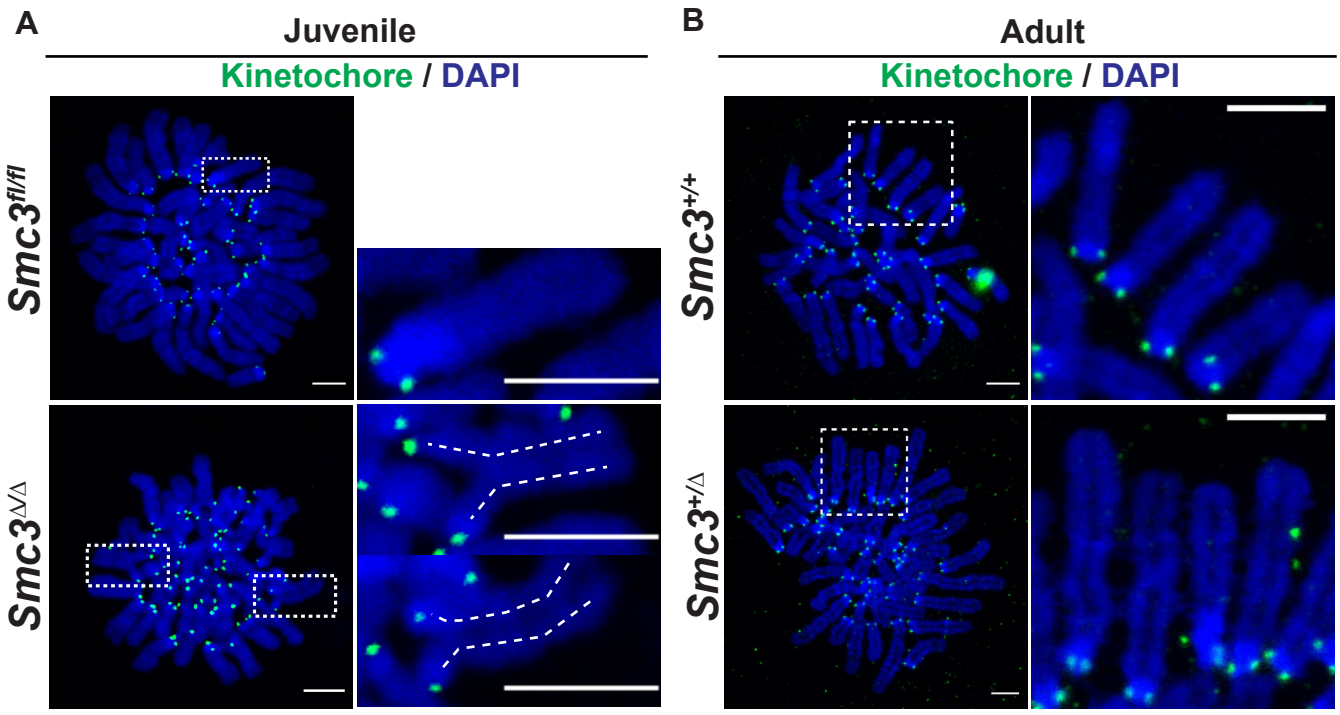

Fig. S8. Loss of maternal *Smc3* disrupts the chromosome structure in zygotes from juveniles. Related to Fig. 7. Zygotes in metaphase were prepared from *Smc3*$^{+/+}$, *Smc3*$^{fl/fl}$, *Smc3*$^{+/fl}$*;Zp3-Cre* (*Smc3*$^{+/\Delta}$) and *Smc3*$^{\Delta/\Delta}$ *cKO* female mice as described in **Fig. 7**. Chromosome spreads were prepared and labeled with CREST (kinetochores, green) and DAPI (DNA, blue) (*n,* juvenile *Smc3*$^{fl/fl}$=1, juvenile *Smc3*$^{\Delta/\Delta}$=4, adult *Smc3*$^{+/+}$=4, and adult *Smc3*$^{+/fl}$*;Zp3-Cre* (*Smc3*$^{+/\Delta}$)=7). Dotted squares indicate the selected area which is shown at increased magnification in the right panel. Dotted lines trace the chromosome arms. Scale bar, 5 µm.

Development • Supplementary information

Source Data

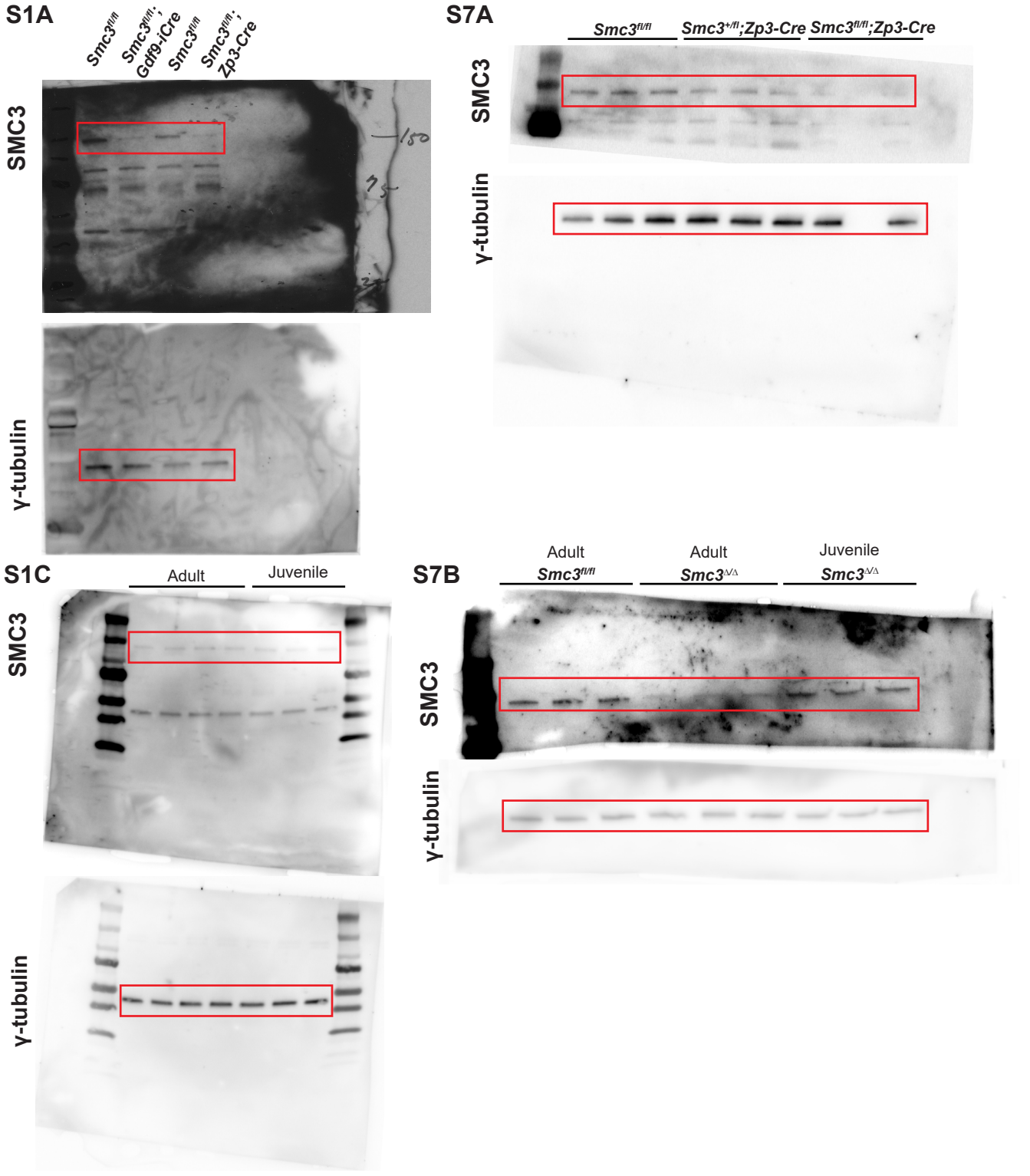

Fig. S9. Source data.

Development • Supplementary information

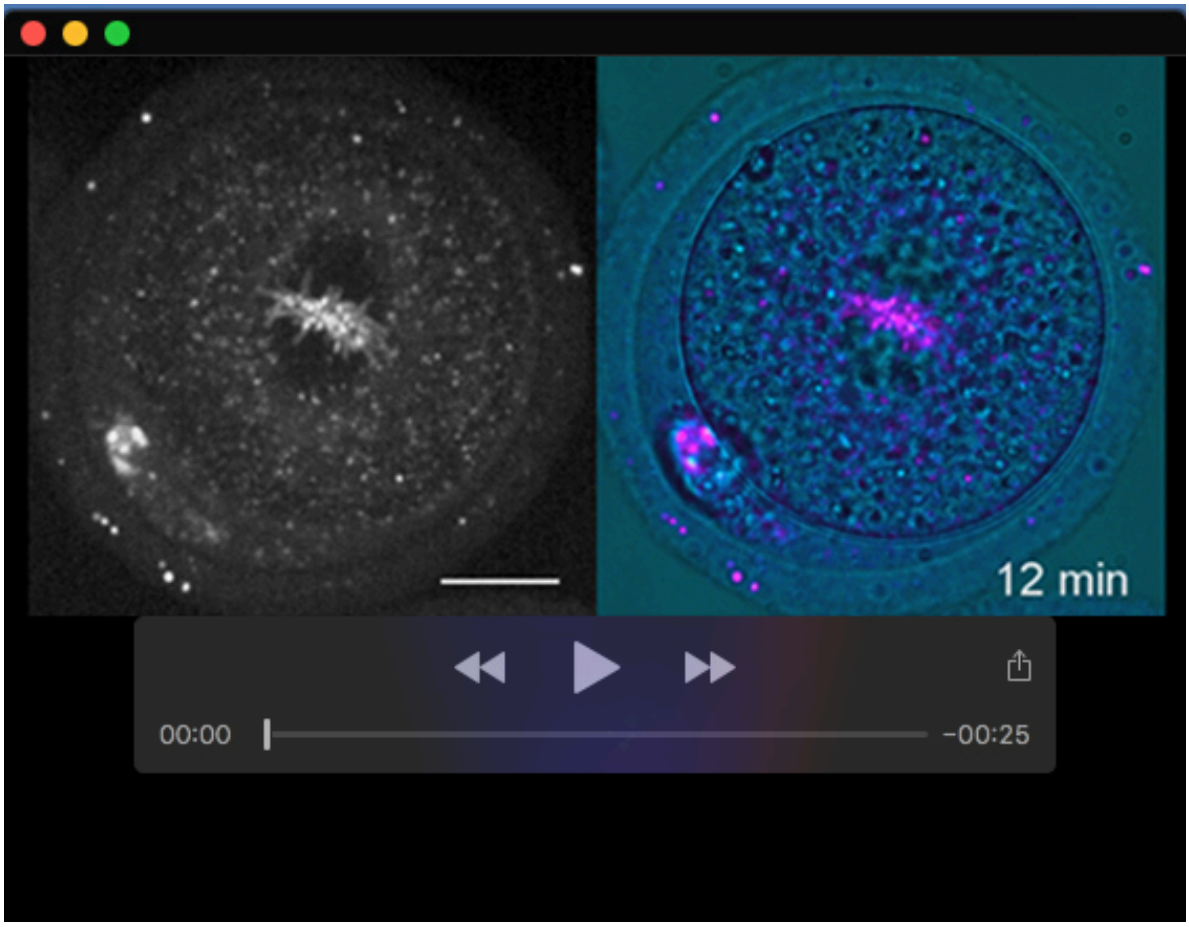

Movie 1. Video of live cell imaging of SIR-DNA dye recording the first mitotic division in *Smc3*$^{fl/fl}$ zygotes. Related to Fig. 4C-E. Left panel shows the SIR-DNA channel and the right panel shows the merged stack of the SIR-DNA channel (magenta) and the widefield channel (cyan). Scale bar, 10 µm.

Development • Supplementary information

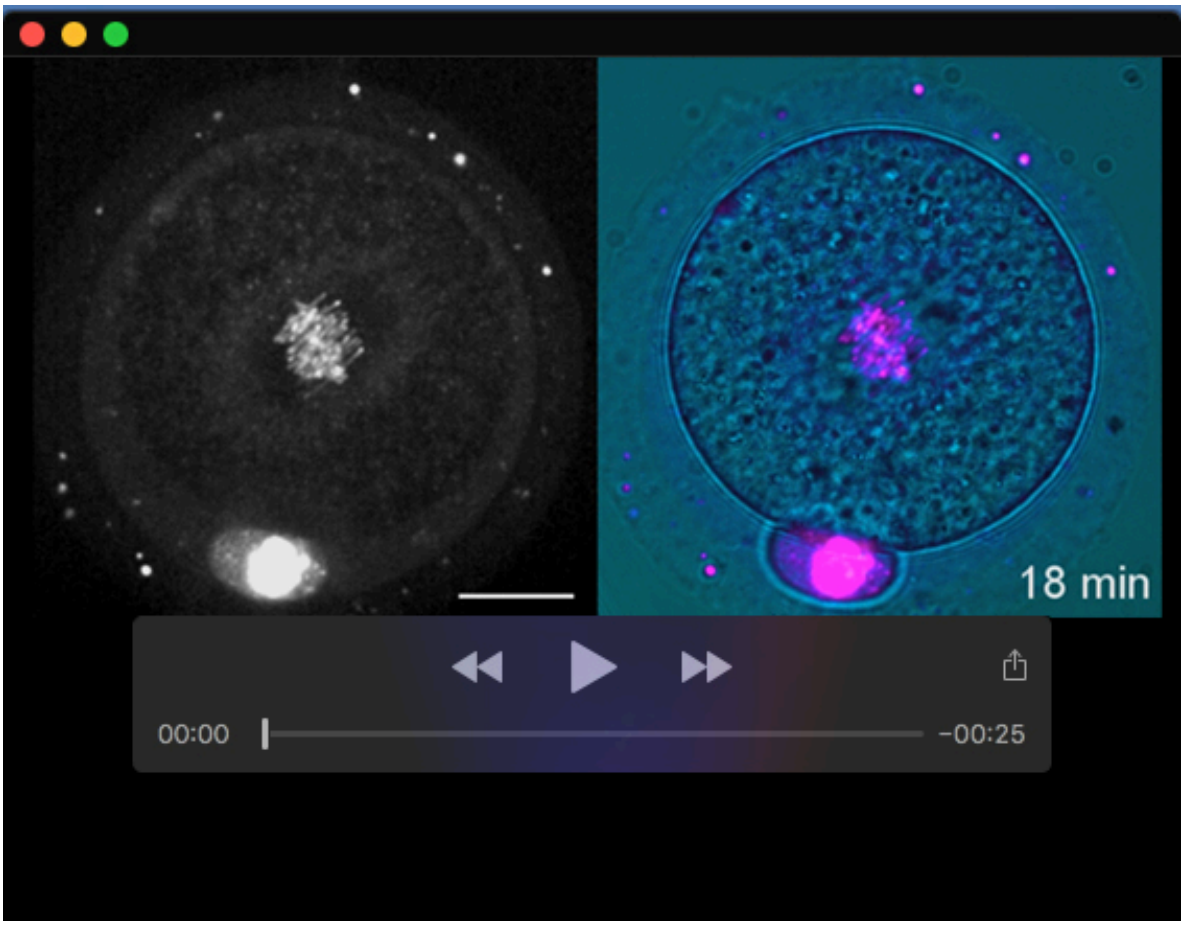

Movie 2. Video of live cell imaging of SIR-DNA dye recording the first mitotic division in *Smc3*$^{\Delta/\Delta}$ *cKO* zygotes. Related to Fig. 4C-E. Left panel shows the SIR-DNA channel and the right panel shows the merged stack of the SIR-DNA channel (magenta) and the widefield channel (cyan). The magenta arrow indicates the micronucleus formed from lagging chromosomes. Scale bar, 10 μm.

Development • Supplementary information